JOURNAL OF GEOPHYSICAL RESEARCH, VOL. 104, NO. D6, PAGES 6101-6121, MARCH 27, 1999

Simulation of upper tropospheric clouds with the Colorado State University general circulation model

Laura D. Fowler and David A. Randall

Department of Atmospheric Science, Colorado State University, Fort Collins

Abstract. We have compared the climatology of upper tropospheric clouds simulated with the Colorado State University (CSU) general circulation model against cloud products retrieved by the International Satellite Cloud Climatology Project (ISCCP). Following the ISCCP cloud classification, upper tropospheric clouds are defined as clouds with cloud tops above 440 hPa. We refined our comparison by considering separately clouds with cloud tops above 180, 310, and 440 hPa in order to exhibit the optical characteristics of the highest clouds in the model and satellite cloud products. Four ranges of visible optical depths (τ) were used to distinguish cirrus ($\tau \leq 3.6$) from optically thicker cirrostratus ($3.6 < \tau \leq 23$) and deep convective clouds ($\tau > 23$) and to further differentiate between thin ($0.02 < \tau \leq 1.6$) and thick ($1.6 < \tau \leq 3.6$) cirrus. Results show that the CSU GCM simulates satisfactorily the zonally averaged distribution of upper tropospheric clouds when all values of τ are included but systematically underpredicts the frequency of occurrence of clouds with values of τ less than 3.6 when compared against ISCCP-D1 data. This result reveals that simulated total-column optical depths for columns that include upper tropospheric clouds are too large relative to satellite-derived values. The CSU GCM simulates upper tropospheric clouds in the tropics more successfully than those in the middle latitudes. In the middle latitudes the model fails to simulate upper tropospheric clouds over the continents, especially over high plateaus and mountain ranges. Discrepancies between the CSU GCM and the ISCCP cloud products can be addressed in terms of our simple formulation of the optical thickness as a function of the prognostic liquid/ice water content, the prescribed value of the effective radius, and the geometrical thickness of the upper tropospheric model layers. We investigate the impact of the vertical resolution used in the GCM on the calculation of the optical depths of single-layer clouds using estimates of the geometrical thickness of cloudy layers from the Lidar In-Space Technology Experiment.

1. Introduction

It has long been recognized that upper tropospheric clouds play a major role in regulating the planetary radiation budget and the atmospheric general circulation, but that in models the impact of these clouds varies depending on the parameterizations of their horizontal area and optical characteristics. It is essential for general circulation models (GCMs) to satisfactorily simulate the climatology of upper tropospheric clouds in order to investigate their interactions with radiation and the general circulation of the atmosphere and to study cloud-climate feedbacks.

Parameterizations of the optical properties of upper tropospheric clouds have been shown to influence not only the top-of-the-atmosphere radiation budget but also the atmospheric circulation simulated by GCMs. Using the National Center for Atmospheric Research (NCAR) Community Climate Model, Version 0, *Ramanathan et al.* [1983] demonstrate that parameterizing the infrared emissivity of cirrus clouds as a function of the liquid/ice water content reduces the equator-to-pole gradient of net radiative heating and improves the simulation of temperatures and zonal winds. The results of *Slingo and Slingo* [1988] corroborate the findings of *Ramanathan et al.* [1983]. Using Version 1 of the Community Climate Model, *Slingo and Slingo* [1988] find that the longwave radiative forcing of nonblack cirrus clouds increases the precipitation maxima at low latitudes and strengthens the Hadley circulation. Experiments conducted by *Ramaswamy and Ramanathan* [1989] on the sensitivity of the atmospheric circulation to solar absorption by cirrus clouds show that enhanced cirrus solar absorption contributes strongly to the stabilization of the upper tropospheric lapse rate by increasing the diabatic heating of the upper troposphere. In the sensitivity studies cited above, the cloud fraction is diagnosed from the large-scale relative humidity, and the computation of infrared emissivity and visible optical depth uses a prescribed (i.e., nonpredicted) distribution of the liquid or ice water paths. In addition to modifying the atmospheric general circulation through radiatively induced feedbacks, the optical properties of upper tropospheric clouds have been shown to influence the sensitivity of climate to a doubling of atmospheric CO_2. *Senior and Mitchell* [1993] demonstrate that the warming-induced increase of liquid water clouds at the expense of ice water clouds leads to a strong negative feedback and that this feedback is enhanced when optical properties are dependent upon the liquid and ice water paths.

Because many contemporary GCMs include a prognostic equation for the mass of condensed water [e.g., *Smith*, 1990; *Ricard and Royer*, 1993; *Tiedkte*, 1993; *Boucher et al.*, 1995; *Del*

Copyright 1999 by the American Geophysical Union.

Paper number 1998JD200074.
0148-0227/99/1998JD200074$09.00

Genio et al., 1996; *Fowler et al.*, 1996; *Rotstayn*, 1997] and because in these models the optical properties of upper tropospheric clouds are interactive and computed as functions of the liquid and ice water paths, it is increasingly important to compare not only the frequency of occurrence and amount of upper tropospheric clouds but also their optical properties against cloud data products. In addition to comparing top-of-atmosphere radiation budget simulations against satellite experiments such as the Earth Radiation Budget Experiment (ERBE) [*Barkstrom*, 1984] and the Cloud and Earth's Radiant Energy System (CERES) [*Wielicki et al.*, 1996], comparing optical properties of upper tropospheric clouds simulated by GCMs against satellite-retrieved products provides an additional tool to assess the ability of models to simulate the global distribution of the ice water path. In contrast to the simulated cloud liquid water path, whose geographical distribution can be compared against cloud liquid water retrieved from satellite microwave radiances over the oceans [*Greenwald et al.*, 1993; *Weng et al.*, 1997], geographical patterns of the vertically integrated ice water path remain unknown, and modelers have been constrained to indirectly estimate the performance of their ice microphysics parameterization [*World Meteorological Organization*, 1995]. Only *Lin and Rossow* [1994] estimated the global distribution of the ice water path from the difference between the International Satellite Cloud Climatology Project (ISCCP) total water path and the special sensor microwave imager (SSM/I) liquid water path for nonprecipitating clouds. One of the objectives of the Tropical Rainfall Measuring Mission (TRMM) [*Simpson et al.*, 1988] is to retrieve the vertical distribution of liquid and ice hydrometeors. Although cloud optical thicknesses are retrieved from top-of-the-atmosphere observed visible radiances by using a radiative transfer model, their use in conjunction with conventional Earth radiation budget data offers an additional path to our understanding of the characteristics of GCM-simulated climates.

Systematic and detailed comparisons between satellite-derived climatologies of upper tropospheric clouds from the ISCCP [*Schiffer and Rossow*, 1983], the high-resolution infrared sounder (HIRS) [*Wylie et al.*, 1994], and the Stratospheric Aerosol and Gas Experiment II (SAGE II) [*Kent et al.*, 1993; *Wang et al.*, 1996] are stimulating the interest of large-scale cloud modelers to compare the geographical distribution and amount of upper tropospheric clouds simulated by GCMs against such satellite cloud products. Disparities between the ISCCP, HIRS, and SAGE II cloud data products can be explained in terms of differences between the field of view and sensitivity of the instruments, which most strongly affect the detection of the thinnest clouds. Among the three climatologies the ISCCP algorithm has the lowest sensitivity to optically thin cirrus, whereas the amount of extrathin cirrus detected by HIRS is quantitatively similar to that detected by SAGE when compared with ISCCP data [*Liao et al.*, 1995]. From matched analyses of 4 months of high-level cloudiness data from HIRS and ISCCP, *Jin et al.* [1996] conclude that about one third of the Earth is covered by high-level clouds, here defined as clouds with tops above the 440-hPa level, and that more than two thirds of these clouds are cirrus, defined as clouds with visible optical depths (τ) less than 3.6. Also, *Jin et al.* [1996] estimate that about half of all cirrus are optically very thin ($\tau <$ 1.3). The abundance of upper tropospheric clouds relative to the observed total cloud amount is a strong motivation to assess the performance of GCMs to simulate this specific cloud type.

Section 2 focuses on the climatology of upper tropospheric clouds from the ISCCP-D1 cloud data products. Our classification of upper tropospheric clouds in four separate ranges of visible optical depths was made using January and July 1990, 1991, and 1992. In sections 3 and 4 we compare the results of a 3-year simulation performed with the Colorado State University (CSU) general circulation model against the satellite-derived cloud climatology. In section 5 we investigate reasons why the CSU GCM fails to simulate some characteristics of the observed upper tropospheric cloudiness. Section 6 summarizes our results and highlights issues to be addressed in future work.

2. The ISCCP-D1 Data

2.1. Description

The ISCCP D-series cloud climatology is the second generation of cloud data products generated by ISCCP, following changes and refinements made to the original cloud detection algorithm [*Rossow et al.*, 1996]. Relative to the first-generation cloud climatology, the C series [*Schiffer and Rossow*, 1991], modifications important to the present study are (1) improved cirrus detection over land, achieved by lowering the infrared threshold from 6 to 4 K, and (2) an improved model for the optical properties of cold clouds (top temperature <260 K) based on the use of an ice polycrystal scattering phase function to retrieve optical depth and top temperature. As explained by *Rossow et al.* [1996], all retrieved parameters such as visible cloud optical thicknesses and cloud-top temperatures are model-dependent quantities, obtained by comparing radiances observed at the pixel level with the results of radiative transfer model calculations. In particular, the retrieved cloud optical properties depend on the microphysical characteristics of the cloud particles used in the radiative transfer model. Visible cloud optical thicknesses are retrieved using two cloud microphysical models. For warm clouds the algorithm uses a liquid water droplet model with a droplet size distribution described by a gamma distribution with a 10-μm mean effective radius and an 0.15 effective variance. For cold clouds, visible optical thicknesses are retrieved using an ice cloud model with a random fractal shape and a -2 power law size distribution from 20 to 50 μm, giving an effective radius of 30 μm and an effective variance of 0.10. The ice crystal model is similar to that investigated by *Minnis et al.* [1993a, b]. More details on the cloud detection algorithm and radiative transfer model are given by *Rossow and Garder* [1993a, b] and *Rossow et al.* [1996], respectively.

In this study we used the D1 product, which is generated by summarizing the pixel-level results and is available every 3 hours on an equal-area map with a 280-km resolution. ISCCP-D1 data provide the geographical distribution of the amount of clouds within a prescribed range of cloud-top pressures and a prescribed range of cloud optical depths. As explained below, every 3-hour map of the cloud amount was first converted to maps of the frequency of occurrence of clouds to match the model diagnostics. Monthly means were computed next. Monthly-averaged equal-area maps of the different cloud variables described below were obtained by computing first the monthly means for each time of day, 0000, 0300, 0600, 0900, 1200, 1500, 1800, and 2100 UTC, and then averaging the hourly-monthly mean values to obtain the monthly mean cloud product. As with the time-averaging technique described by *Rossow et al.* [1996], hourly-monthly means based on less than three daily observations were excluded from the monthly mean

Table 1. Classification of Upper Tropospheric Clouds as Functions of the Visible Optical Depth

Cloud Category	Optical Depth
All clouds	$0.02 < \tau \leq 378.7$
All cirrus	$0.02 < \tau \leq 3.6$
Thick cirrus	$1.3 < \tau \leq 3.6$
Thin cirrus	$0.02 < \tau \leq 1.3$

calculations, but in contrast to *Rossow et al.* [1996], we did not make any adjustment to the hourly-monthly mean data sets before averaging over the time of day and we did not apply any diurnal sampling adjustment to the monthly mean. As explained by *Rossow et al.* [1996], the diurnal sampling adjustment has a small effect on monthly-averaged products when visible light spectrometer VIS/IR radiances are used, which is the case for upper tropospheric clouds. Indeed, comparison of our monthly-averaged upper tropospheric cloud amount against that of the stage-D2 cloud product (the monthly-averaged ISCCP-D1 quantities) did not reveal any systematic bias in our monthly means. Each equal-area map was later converted to an equal-angle map with 2.5° × 2.5° latitude-longitude resolution and then further interpolated to the CSU GCM's 4° × 5° grid.

Following the ISCCP radiometric cloud classification [*Schiffer and Rossow*, 1991], clouds with cloud-top pressures less than 440 hPa are labeled as high-level clouds, and cirrus are defined as high-level clouds whose visible optical depths are less than 3.6. Using ISCCP-D1 daytime only products, which are, of course, the only products containing information on the visible optical depths, we consider separately high-level clouds with cloud-top pressures less than 180, 310, and 440 hPa. Here it is important to add that this classification is cumulative, meaning that clouds with cloud-top pressures less than 440 hPa may, for instance, also include clouds with cloud tops less than 310 and 180 hPa. For each cloud-top pressure we also consider four ranges of visible optical depths (τ), as shown in Table 1. When using the *McClatchey et al.* [1972] standard atmospheres, 440 hPa corresponds to an altitude of 6.9 km in the tropics and 6.8 km (6.4 km) in the summer (winter) middle latitudes. A pressure of 310 hPa corresponds to an altitude of 9.4 km in the tropics and 9.3 km (8.2 km) in the summer (winter) middle latitudes. Finally, 180 hPa is equivalent to a height of 13.1 km in the tropics and to a height of 13 km (12.3 km) in the summer (winter) middle latitudes.

The "all-clouds" type refers to high-level clouds regardless of τ, which besides cirrus also includes cirrostratus as well as deep convective clouds. The all-cirrus type refers to high-level clouds for which τ is greater than 0.02 and less than 3.6, as in the ISCCP radiometric cloud classification. The all-cirrus category is further divided into two classes. The thick-cirrus category includes cirrus whose τ is greater than 1.3 but less than 3.6, and the thin-cirrus category includes cirrus whose τ is less than 1.3 but greater than 0.02. Here 0.02 is the detection threshold of the ISCCP algorithm, expressed in terms of visible optical depth.

As explained in the next section, the CSU GCM does not include a parameterization of fractional cloudiness at this time. The cloud amount is equal to 0 or 1 and fills the entire model grid box, depending upon the amount of condensate present in the box. When using the definition above, it is actually more accurate to refer to the simulated monthly-averaged cloud amount as a mean frequency of occurrence of clouds. In contrast, ISCCP-D1 data define the cloud amount as the horizontal fraction of a 2.5° × 2.5° box covered by clouds. In order to compare simulated and observed cloud diagnostics, we converted the ISCCP-D1 cloud amount variable (later referred to as A) into an ISCCP-D1 frequency of occurrence (later referred to as f) to match the simulated cloud amount variable. For a given cloud variable, A is defined as the number of cloudy pixels with the same cloud property (for instance, cloud-top pressure, visible optical depth) divided by the total number of pixels in an equal-area grid. By definition, f is equal to 1 if A is greater than zero in a given grid box, and f is equal to 0 otherwise. As seen in Figure 1, there are significant differences between the magnitudes of A and f for cloud-top pressures less than 180 hPa. The monthly-averaged f shows geographical patterns similar to those of the monthly-averaged A, but the magnitude of f is, of course, several times greater than that of A. Similar differences between the monthly-averaged A and f are seen for clouds with lower cloud-top pressures. (Maps of A and f for clouds with cloud tops lower than 310 and 440 hPa are omitted for brevity.) This significant difference between the magnitudes and global distributions of A and f illustrates the necessity of converting A provided in the ISCCP-D1 data to f for objective comparisons against the CSU GCM cloud products, as well as the importance of including a parameterization of fractional cloudiness in the near future. Adding a parameterization of the fractional cloudiness to the CSU GCM will help to simulate the cloudy fraction of the GCM grid box and allow a direct comparison of the monthly averaged upper tropospheric cloudiness against ISCCP data. This direct comparison between simulated and satellite-derived cloud products cannot be made at present. In converting A to f, we also emphasize that this study aims at assessing the ability of the cloud formation process parameterized in the CSU GCM to generate clouds with realistic frequencies where they are actually observed, and not the ability of our parameterization to generate the actual fractional cloudiness, which it cannot do at present.

2.2. Interannual Variability

We investigated the observed year-to-year variability in the frequency of occurrence of all clouds between January 1990, 1991, and 1992 and July 1990, 1991, and 1992, whose ensemble averages are used to assess the performance of the CSU GCM to simulate the amount and optical properties of high-level clouds. Here our motivation is to ensure that the natural year-to-year variability in the ISCCP data relative to the 3-year mean does not bias our comparison between the model and the satellite data. As an example, Figure 2 shows the zonally averaged departure of f for each January (July) from the January (July) 3-year mean, for the all-clouds category with cloud tops less than 440 hPa. The year-to-year variability of all clouds is significant at all latitudes, with absolute zonally averaged variations as large as 15–20%. January and July 1990 show above-average values of f, whereas January and July 1992 systematically exhibit below-average values of f, at all latitudes. In 1991, and in contrast to the other 2 years, the departure of f from its 3-year average is positive in January but negative in July. We have found that the year-to-year variability is also larger for all clouds with cloud tops above 180 and 310 hPa than for all clouds with cloud tops above 440 hPa. Maps of the geographical distribution of the departure of f for each January (July) from the ensemble mean did not reveal any preferred centers

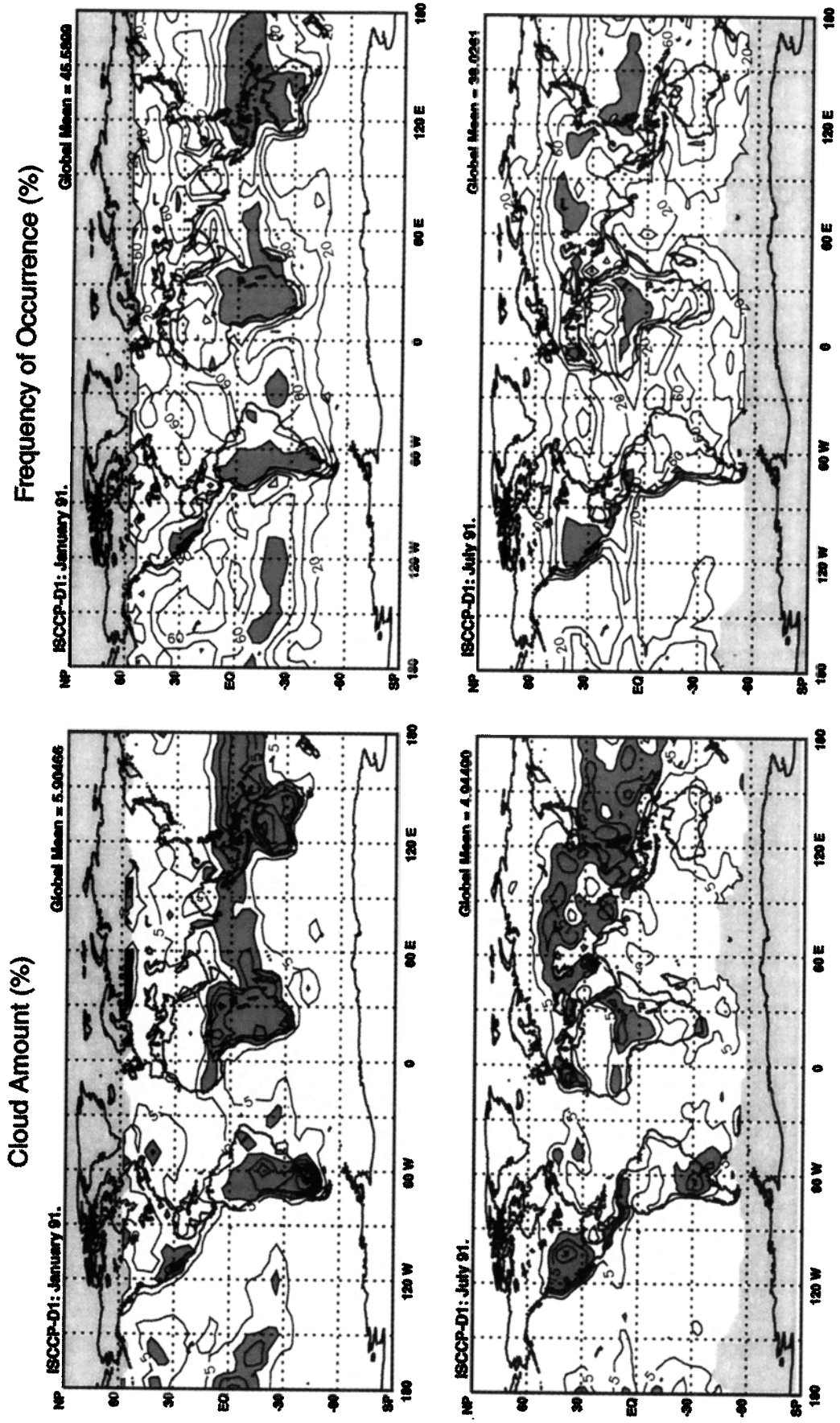

Figure 1. Geographical distribution of (left panels) the cloud amount versus (right panels) the frequency of occurrence of International Satellite Cloud Climatology Project (ISCCP-D1) all clouds with cloud-top pressures less than 180 hPa. The top two panels are for January, and the bottom two panels are for July. Units are in percent. Left panels have contour intervals every 10%, and shading corresponds to values greater than 20%. Right panels have contour intervals every 20%, and shading corresponds to values greater than 80%.

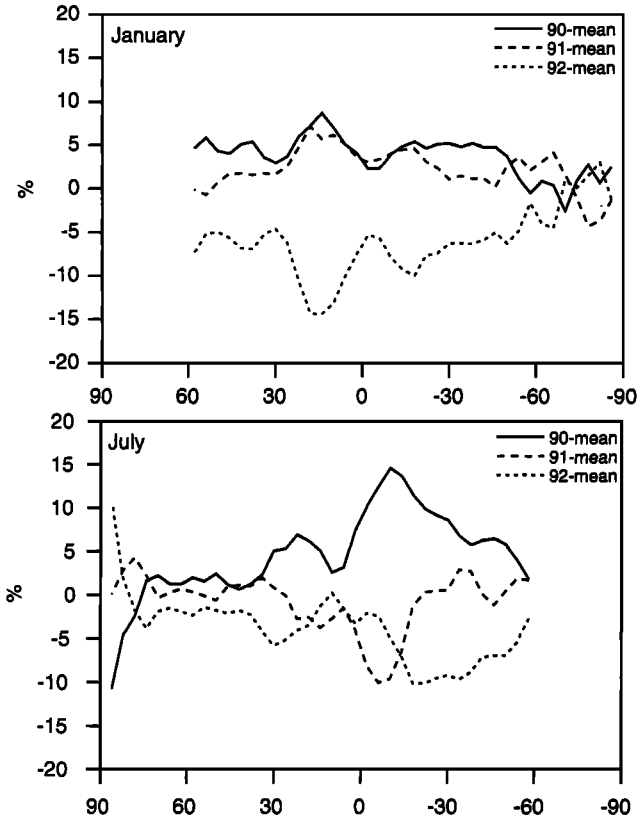

Figure 2. Zonally averaged profile of the difference in the frequency of occurrence of ISCCP-D1 all clouds with cloud-top pressures less than 440 hPa between each individual January (July) and the January (July) 3-year mean. Units are in percent.

of interannual variability. These maps are omitted here for brevity. In 1990 an increase in f is observed at all latitudes, but it appears to be larger over the oceans than over the continents. In 1992 the decrease in f is also more pronounced over the oceans, especially over the subtropical Pacific Ocean. It would certainly be very interesting to investigate in greater detail causes of the year-to-year variability of f for all clouds, but since the objective of this research is to analyze the ability of the CSU GCM to simulate upper tropospheric clouds, such an investigation is beyond the scope of the present study.

2.3. Results

We now discuss the monthly-averaged frequencies of occurrence of clouds computed from the ISCCP-D1 data. Figure 3 shows the zonally averaged distribution of f for the four cloud categories with cloud-top pressures above 180, 310, and 440 hPa for January. Here "January" refers to the ensemble average for January 1990, 1991, and 1992. Figure 4 is the same as Figure 3 but for July, where "July" refers to the July ensemble average over the same 3 years. Global averages of f for the four different cloud types are listed in Table 2, for January and July.

The zonally averaged profile of f for all clouds is significantly different between January and July. In July, f exhibits one narrow primary maximum along the Intertropical Convergence Zone (ITCZ) just north of the equator and three broader secondary maxima, one located in the winter hemisphere at about 40°S and two located in the summer hemisphere between 30°N and 60°N. For clouds with cloud-top pressures less than 180 hPa these two summer maxima collapse into one maximum located at about 40°N. In contrast, in January, f for all clouds displays one wide primary maximum that straddles the equator between about 5°N and 30°S, flanked by two secondary maxima, a winter maximum located over the middle latitudes and a summer maximum located at about 70°S. For high-level clouds with cloud-top pressures less than 180 hPa, the secondary summer maximum is not seen.

As shown in Figures 3 and 4, the contributions of all cirrus, thick cirrus, and thin cirrus to the zonally averaged distribution of all clouds vary with latitude and cloud-top pressure. First, it is obvious that the all-cirrus category contributes strongly to the all-clouds category regardless of the cloud-top pressure (91.7% in January and 92.2% in July for cloud tops less than 440 hPa), meaning that upper tropospheric clouds preferably have visible optical depths less than 3.6. The fact that satellite-derived upper tropospheric clouds with optical depths less than 3.6 are so abundant is an additional motivation to test the performance of our GCM. It is also evident that thin cirrus contribute a major part to the all-cirrus category at all latitudes

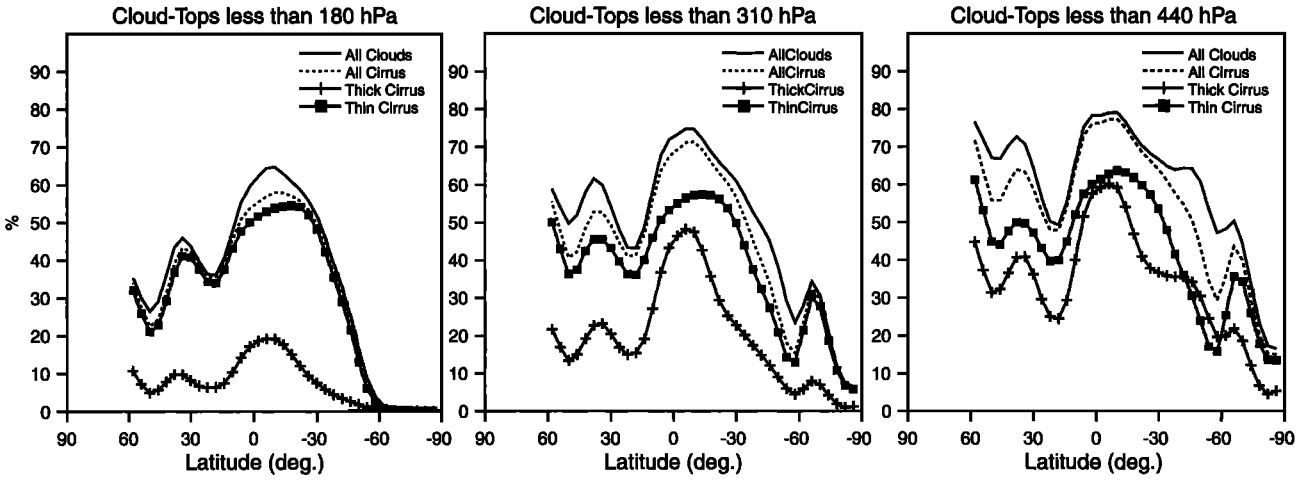

Figure 3. Zonally averaged profile of the frequency of occurrence of ISCCP-D1 upper tropospheric clouds with cloud-top pressures less than 180, 310, and 440 hPa, in January. Units are in percent.

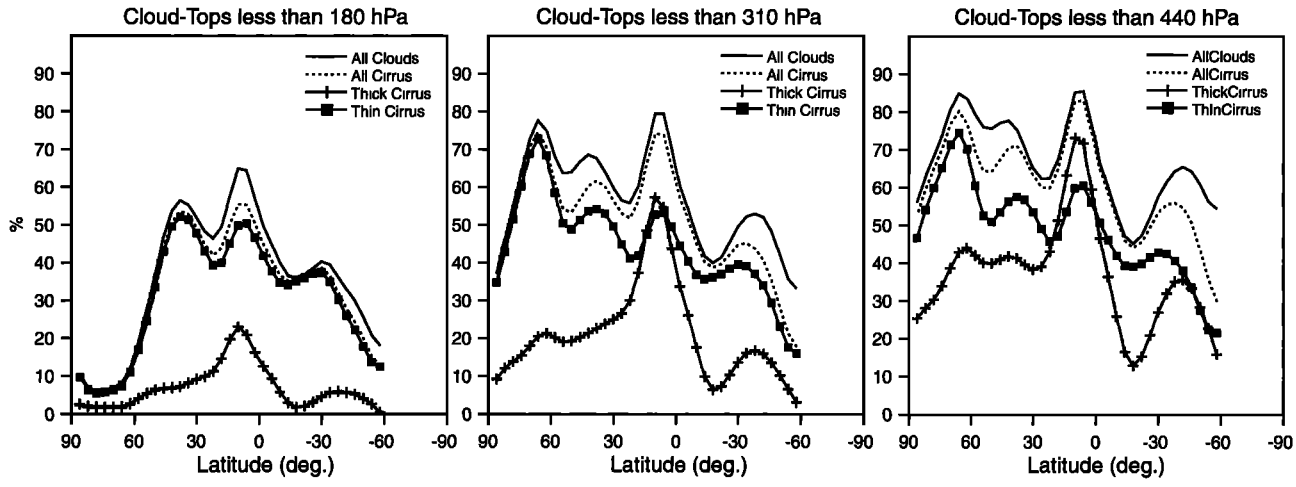

Figure 4. Same as Figure 3, but for July.

in both January and July (79.5% in January and 79.1% in July for cloud tops less than 440 hPa). Finally, and in contrast to thick cirrus, whose magnitudes strongly increase when their cloud-top pressures vary from 440 to 180 hPa, especially in the tropics, the frequency of thin cirrus does not significantly change between 180 and 440 hPa. This suggests that besides being the highest and most abundant type of upper tropospheric clouds, thin cirrus also have longer lifetimes than thick cirrus. Thin cirrus form in two distinct regimes: an optically thin upper tropospheric shield associated with jet stream activity in extratropical latitudes and thin debris from deep convective activity in the tropics. In contrast, thick cirrus constitute more massive debris from tropical anvils that form at the tops of cumulonimbus towers.

Differences in the geographical distribution of f between thick cirrus and thin cirrus are clearly shown in Figures 5 and 6 for January and Figures 7 and 8 for July. As seen in Figures 5 and 7, thick cirrus are most abundant along the ITCZ over the eastern Pacific and Atlantic Oceans and over the well-known convectively active regions of Central America and equatorial Africa in July and South America and southern Africa in January. Thick cirrus also have a strong signature over the warm pool region of the western Pacific Ocean, as well as over the Indian Ocean. In July, thick cirrus with cloud-top pressures less than 440 hPa extensively cover Asia and the southern part of North America. They are also found over the cyclogenetic regions along the western sides of the North Atlantic and North Pacific Oceans. As also shown in Figures 5 and 7, the frequency of occurrence of thick cirrus decreases rapidly with decreasing cloud-top pressures. For cloud-top pressures less than 180 hPa, thick cirrus are confined to the deep convective activity regions over the tropics.

In contrast to Figure 5 (Figure 7), Figure 6 (Figure 8) reveals little variation with height in the geographical distribution of f for thin cirrus, with cloud-top pressures varying between 180 and 440 hPa, reinforcing the idea that thin cirrus are confined to the vicinity of the tropopause. In contrast to thick cirrus, thin cirrus are poor markers for the location of the ITCZ and deep convection over the continents, simply because thin cirrus cover a major part of all continents. Their frequency of occurrence is a maximum over mountain ranges as well as over the western Pacific Ocean, indicating that orographic lifting plays a major role in the formation of optically thin upper tropospheric clouds.

3. Model Description

The version of the CSU GCM used here is a 17-level grid-point model with a horizontal grid spacing of 4° in latitude and 5° in longitude. The dynamics and physics of the GCM are the same as the ones used by *Fowler et al.* [1996], except that the earlier parameterization of moist convection [*Pan and Randall*, 1998], consisting of a modified version of the Arakawa-Schubert scheme [*Arakawa and Schubert*, 1974] (see also *Lord* [1982] and *Lord et al.* [1982]), was replaced by the parameterization of *Ding and Randall* [1998]. In contrast to the Arakawa-Schubert parameterization in which cumulus updrafts originate only at the top of the planetary boundary layer (PBL), the parameterization of *Ding and Randall* [1998] allows multiple cloud-base levels and uses a linear (rather than exponential)

Table 2. Globally Averaged Frequency of Occurrence of ISCCP-D1 Upper Tropospheric Clouds by Cloud Type, for January and July

	January			July		
Cloud Type	180 hPa	310 hPa	440 hPa	180 hPa	310 hPa	440 hPa
All clouds	41.4	55.2	65.3	41.4	57.8	66.4
All cirrus	38.3	50.1	59.9	37.6	52.3	61.2
Thick cirrus	9.1	23.8	38.3	8.2	23.6	38.6
Thin cirrus	36.3	42.4	47.6	35.6	44.1	48.4

Values are given in percent.

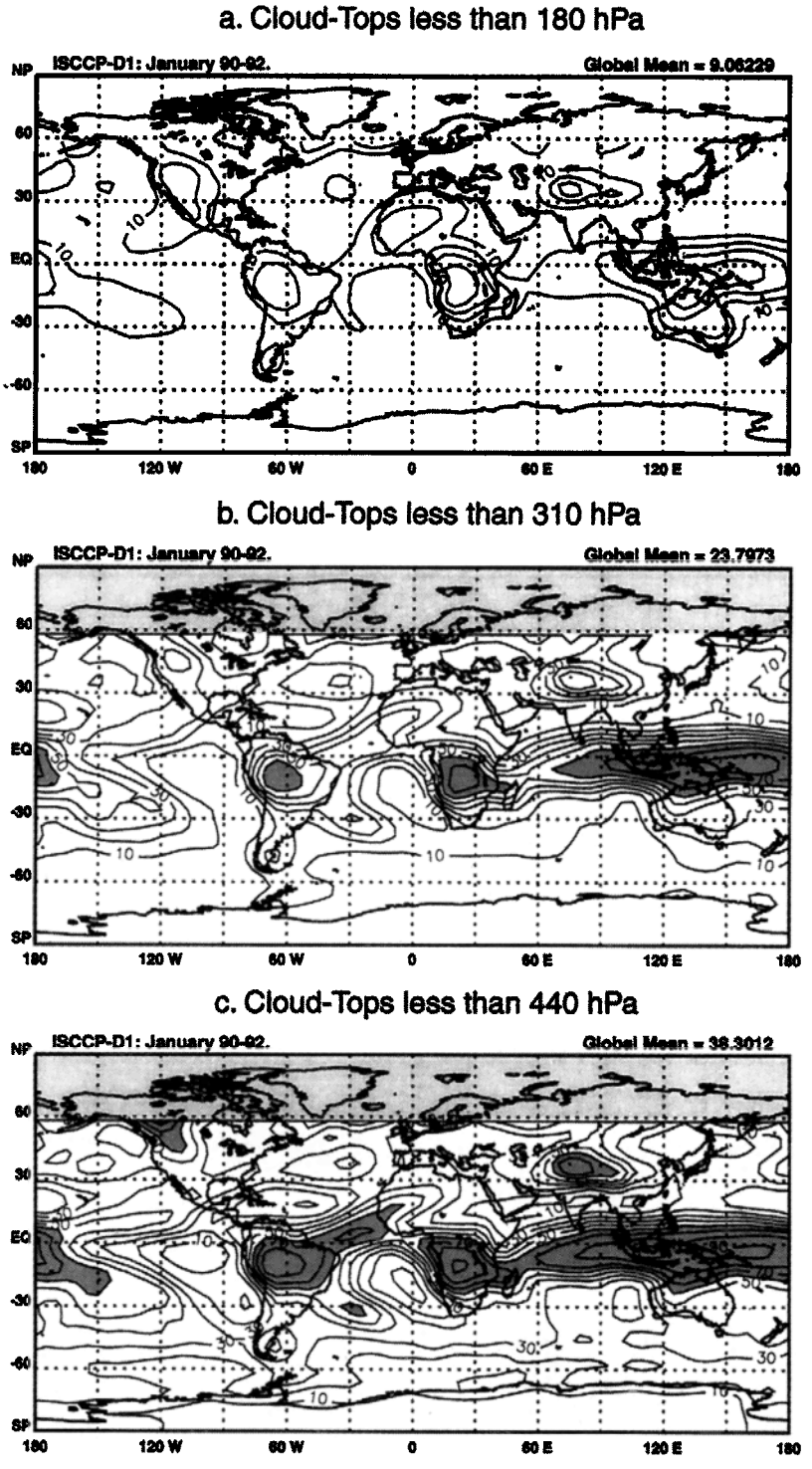

Figure 5. Geographical distribution of the frequency of occurrence of ISCCP-D1 thick cirrus with cloud-top pressures (a) less than 180 hPa, (b) less than 310 hPa, and (c) less than 440 hPa in January. Units are in percent, and contour intervals are every 10%. Shading corresponds to values greater than 60%.

profile of the cumulus mass flux for each cloud type. Differences in the simulated climate between the two parameterizations have been analyzed by *Ding and Randall* [1998]. They concluded that although the precipitation pattern produced with a linear mass flux was smoother, the large-scale dynamics and thermodynamics were not drastically changed relative to those produced by the original Arakawa-Schubert parameterization.

In the CSU GCM the fractional area occupied by convective updrafts is assumed to be small enough so that their radiative effects are negligible. All radiatively active clouds are large-scale clouds whose formation can be triggered by two physical

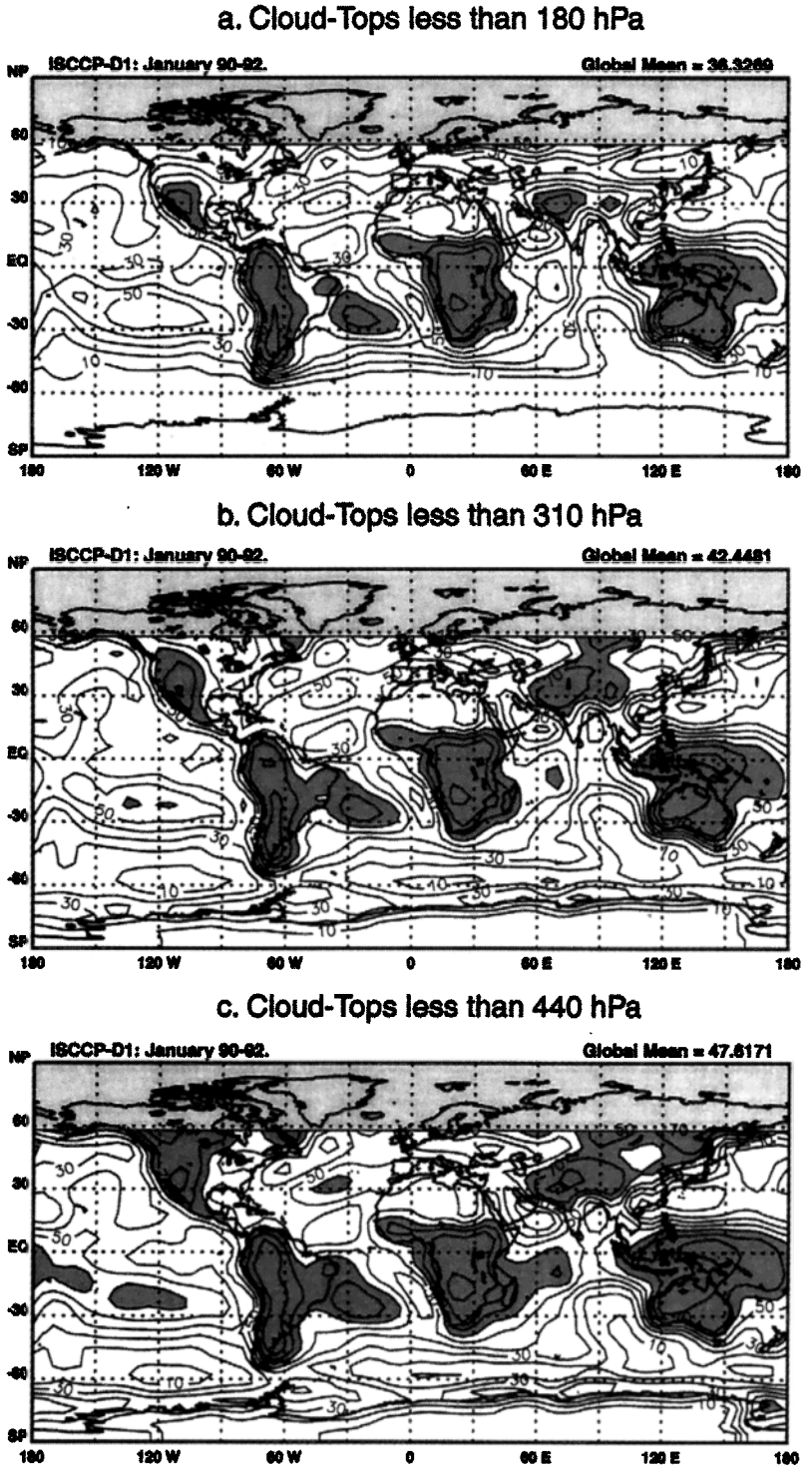

Figure 6. Geographical distribution of the frequency of occurrence of ISCCP-D1 thin cirrus for cloud-top pressures (a) less than 180 hPa, (b) less than 310 hPa, and (c) less than 440 hPa, in January. Units are in percent, and contour intervals are every 10%. Shading corresponds to values greater than 60%.

processes only: (1) detrainment of cloud water and cloud ice at the tops of cumulus towers and (2) large-scale condensation. Clouds are not allowed to form in the two highest model layers, which are located between 100 hPa and the model's top, fixed at 51.3 hPa. The CSU GCM includes five prognostic equations for the mass of water vapor, cloud water, cloud ice, rain, and snow, and interactions between the five water species are parameterized using bulk cloud microphysics equations [*Fowler et al.*, 1996]. Nevertheless, the model does not include fractional cloudiness at this time. Except for PBL clouds for which the formulation of *Harshvardhan et al.* [1989] is used, the cloud fraction is equal to 1 when and where the total amount of

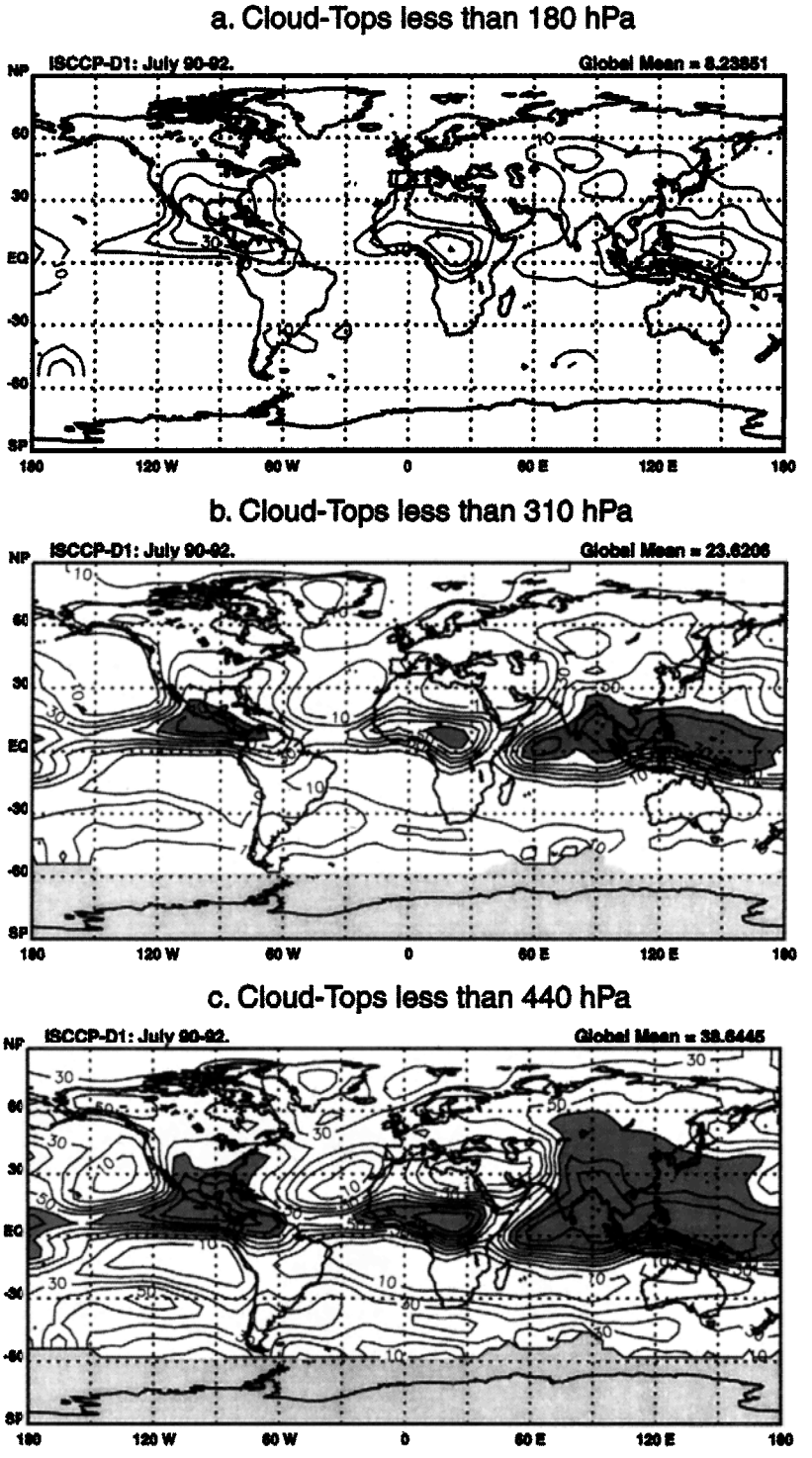

Figure 7. Same as Figure 5, but for July and for thick cirrus.

condensate exceeds 10^{-5} kg kg^{-1}. As explained by *Fowler and Randall* [1996], this finite threshold is necessary to avoid the widespread formation of optically very thin upper tropospheric clouds and will be removed when the parameterization of fractional cloudiness is implemented.

Explicit simulation of the amount of cloud water, cloud ice, rain, and snow suspended in the atmosphere allows cloud optical properties to be interactive and dependent on the water path. As described by *Fowler and Randall* [1996], the optical depth of a model layer is equal to the sum of the optical depths of cloud water (τ_c), cloud ice (τ_i), and snow (τ_s) in the temperature range where the three water species are allowed to coexist and is equal to the optical depth of each individual species otherwise. The computation of τ_x, where x refers to the subscript c for cloud water, i for cloud ice, and s for snow, follows the formulation of *Stephens* [1978]:

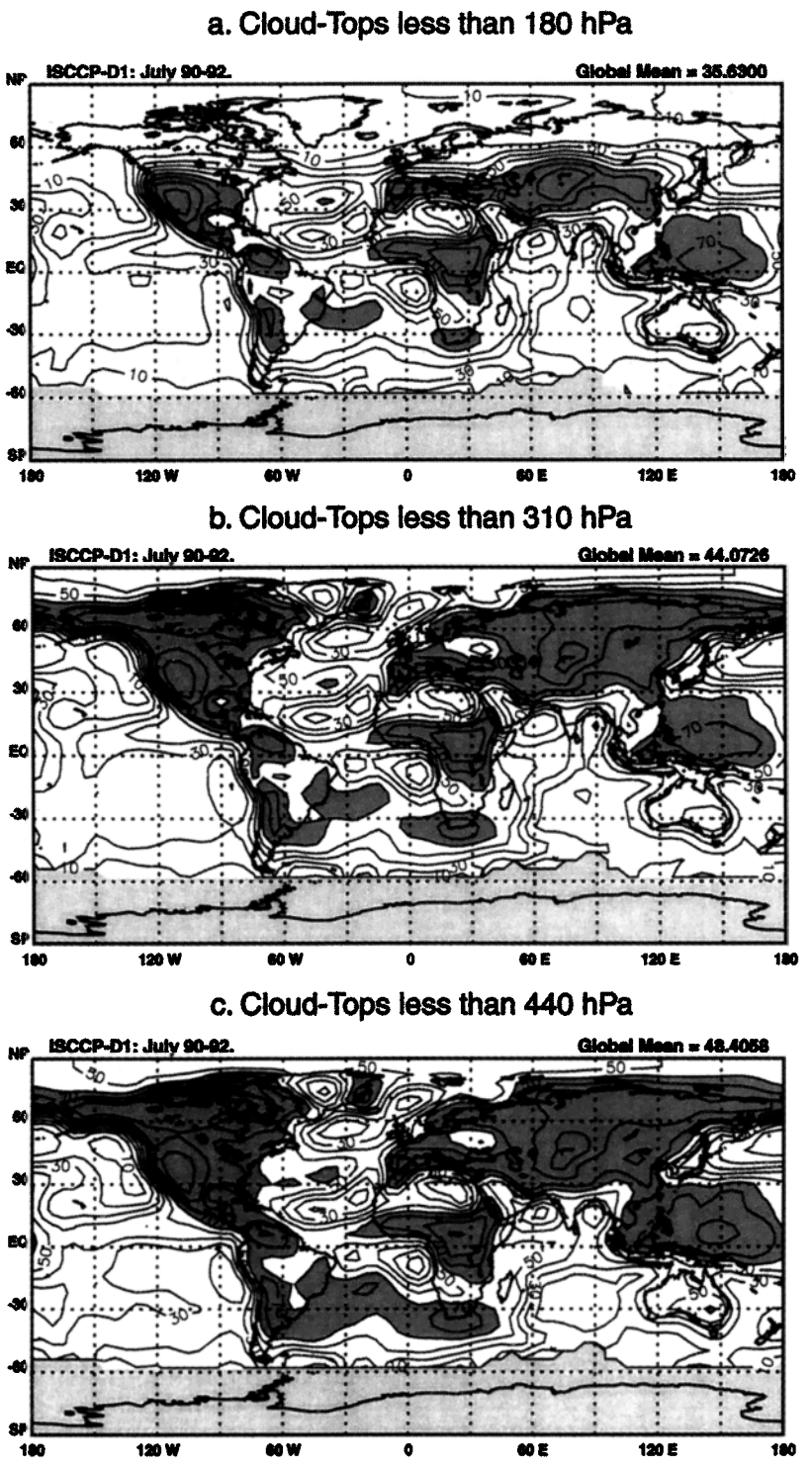

Figure 8. Same as Figure 6, but for July and for thin cirrus.

$$\tau_x = \frac{3}{2}\frac{W_x}{r_e} \qquad W_x = w_x \rho \Delta z, \tag{1}$$

where W_x is the cloud water, cloud ice, or snow path (with dimensions of g m^{-2}) and r_e is the effective radius (in micrometers). W_x is itself a function of the cloud water, cloud ice, or snow mixing ratio (w_x) times the air density (ρ) times the vertical depth of the cloud (Δz). Here r_e is set equal to 10 μm for cloud water, 30 μm for cloud ice, and 1000 μm for snow. In the CSU GCM, and except for PBL clouds whose cloud depth can vary continuously, a cloud occupies the whole depth of a model layer, so that it is easy to depict the base and top levels of a cloud column if that column fills several consecutive model layers, as well as to distinguish between clear-sky and cloudy layers. For satellite-derived cloudiness, cloud base information is not available, and the retrieved optical depth is that of the

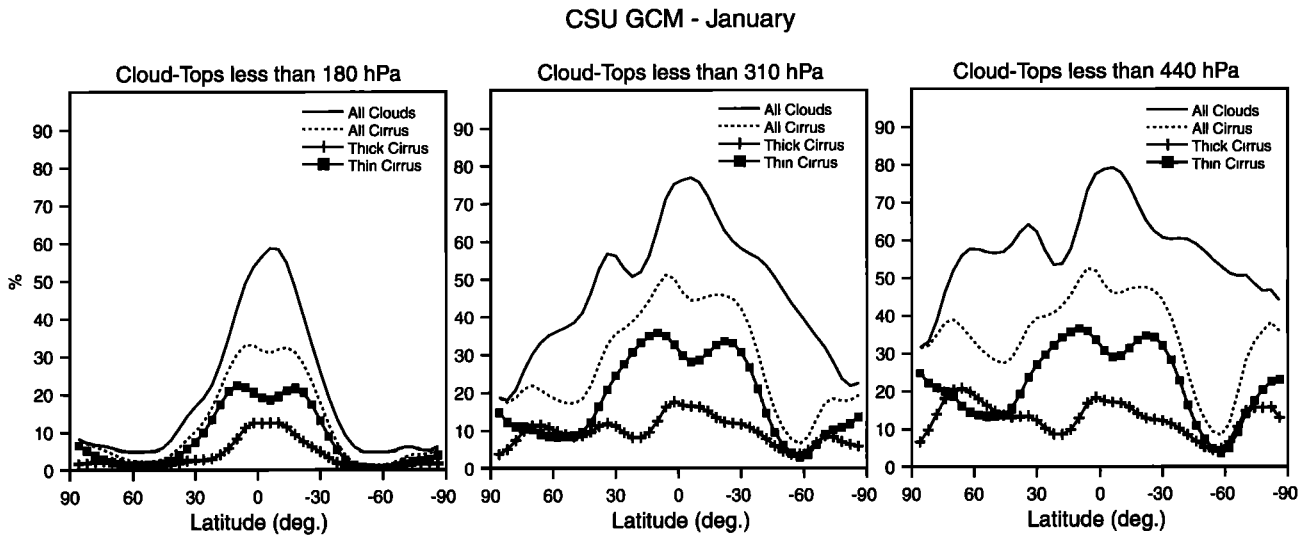

Figure 9. Zonally averaged profile of the frequency of occurrence of simulated upper tropospheric clouds with cloud-top pressures less than 180, 310, and 440 hPa, in January. Units are in percent.

whole atmospheric column as seen from the satellite, regardless of the vertical arrangement of individual cloud layers. In order to match the classification of f by ranges of ISCCP-D1 optical depths, the simulated visible optical depths discussed here are optical depths of atmospheric columns which are capped by clouds with cloud-top pressures less than 180, 310, or 440 hPa.

As for the ISCCP-D1 data, we investigated the year-to-year variability of f as simulated by the CSU GCM. Interannual variability in the model resulted solely from random atmospheric fluctuations, because climatological seasonally varying sea surface temperatures were used. Zonally averaged differences of f between individual months and their respective 3-year averages revealed absolute values less than 3%, regardless of the cloud-top pressure considered, and maps of the departure of f relative to its 3-year mean did not reveal any preferred geographical location with systematic large year-to-year variability. We conclude that our results make up a representative picture of simulated upper tropospheric clouds in the CSU GCM.

4. Results

Figures 9 and 10 show the same classification of upper tropospheric clouds as Figures 3 and 4, but this time for clouds simulated by the CSU GCM. The simulated cloud classification exhibits several significant differences and some similarities when compared against its ISCCP-D1 counterpart.

On the negative side, the CSU GCM fails to simulate the two observed July extratropical maxima of clouds with cloud-top pressures less than 180 hPa. At lower cloud-top pressures, only the all-clouds category displays two extratropical maxima, whose magnitudes are nevertheless weaker than those seen in Figures 3 and 4. The double-peak structure of the observed all-clouds f seen in the northern hemisphere in July is also missing. The same disagreement between satellite-derived and

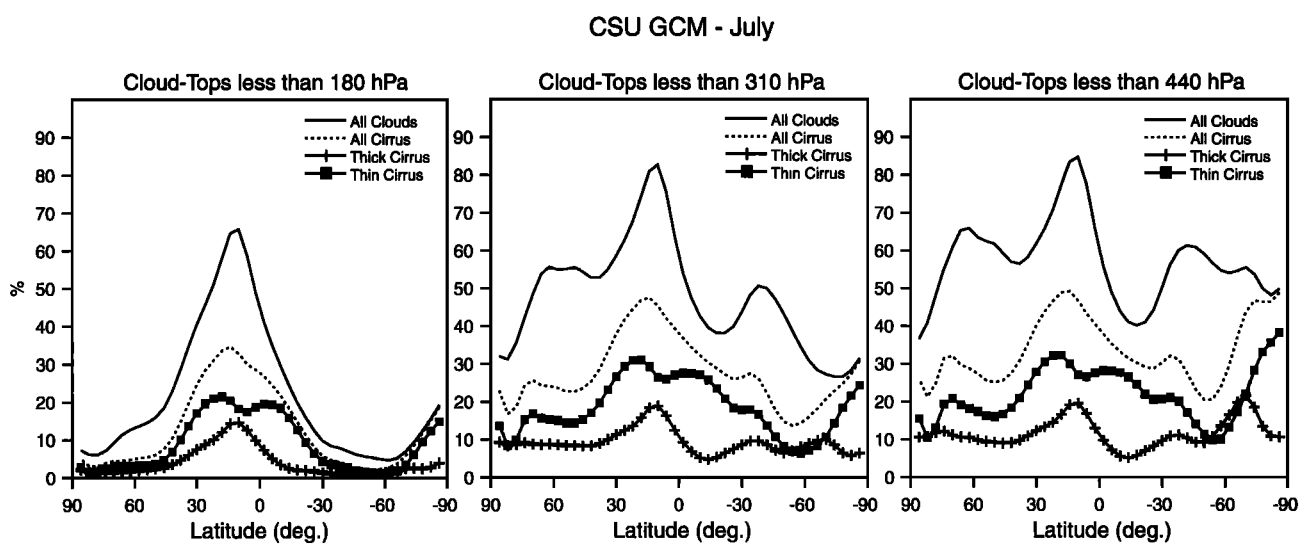

Figure 10. Same as Figure 9, but for July.

simulated upper tropospheric clouds is also seen in January. On the positive side, the CSU GCM reproduces reasonably well the maxima of all clouds along the ITCZ, but the simulated width of this feature is broader than observed, especially in July.

In terms of classification by ranges of optical depths the CSU GCM has a tendency to produce upper tropospheric clouds that are optically too thick when compared against the ISCCP-D1 cloud climatology. As shown in Figures 9 and 10, the amount of all cirrus relative to the amount of all clouds is too small when compared against the satellite-derived cloudiness, meaning that the simulated upper tropospheric clouds have a preferred visible optical depth greater than 3.6, following the classification of Table 1. This deficiency is also revealed in that the zonally averaged distribution of all cirrus remains relatively constant between upper tropospheric clouds with cloud-top pressures less than 180, 310, and 440 hPa. This is in contrast to the satellite-observed clouds, for which the increase in all clouds between 180 and 440 hPa results from an increase in clouds with visible optical depths less than 3.6, while that of the corresponding simulated all clouds results from an increase in clouds with visible optical depths mostly greater than 3.6. Finally, in contrast to the satellite-derived tropical thick cirrus, whose frequency of occurrence increases when their cloud-top pressures vary from 440 to 180 hPa, and the observed tropical thin cirrus, whose frequency of occurrence remains relatively constant regardless of the cloud-top pressure, the frequencies of occurrence of both simulated tropical thick and thin cirrus increase with decreasing cloud-top pressure.

Before we focus our discussion on the simulated global distributions of thick and thin cirrus and comparisons with the satellite data, we investigate differences between the global distributions of simulated and observed all clouds and all cirrus with cloud-top pressures less than 440 hPa, as shown in Figure 11. As already pointed out when comparing Figure 9 against Figure 3 for January and Figure 10 against Figure 4 for July, the CSU GCM underestimates the frequency of occurrence of all clouds and all cirrus in both months. The globally averaged difference in all cirrus between the model and observations reaches values as high as -22.5% in January and -27.1% in July, whereas that in all clouds is -3.4% in January and -7.5% in July. It is interesting to note that the globally averaged difference between the simulated and observed all-clouds type increases with decreasing cloud-top pressures, indicating that the CSU GCM has difficulty in simulating upper tropospheric clouds at the highest levels.

The bottom panels in Figure 11 show that the frequency of occurrence of all clouds is strongly underestimated over the continents and, in particular, over the tropical convectively active regions and mountain ranges. Overestimation of the occurrence of upper tropospheric clouds is seen mostly over the oceans, in particular over the Pacific and Indian Oceans as well the North Atlantic Basin, especially in July. Comparing the January versus July difference maps for the frequency of occurrence of simulated and satellite-observed all clouds reveals that the seasonal cycle of all clouds simulated with the CSU GCM over the oceans is less than observed. The overestimation in the frequency of occurrence of simulated all clouds is greater in January than in July over Central America, where ISCCP-D1 data show a minimum in all clouds in January. The monthly-averaged difference in all clouds between the model and satellite data is greater in July than in January over the Pacific Convergence Zone, where ISCCP-D1 data show a minimum in all clouds in July. This result indicates that the CSU GCM is unable to simulate the seasonal shift of the well-known areas of upper tropospheric cloudiness associated with deep convection. The January difference map also shows that the CSU GCM overestimates the frequency of occurrence of all clouds over the Southern Ocean.

Of greater concern is the difference in the geographical distribution of all cirrus between the CSU GCM and ISCCP-D1 data. As seen in Figure 11, the frequency of occurrence of all cirrus is systematically underestimated relative to the observations, except for a few areas over the oceans. In July the model overestimates the incidence of all cirrus on each side of the ITCZ in the Pacific Ocean as well as along the ITCZ over the Atlantic Ocean. In January the frequency of occurrence of all cirrus is overestimated over the Indian Ocean, the western Pacific Ocean below 30°S, and along both coasts of Central America.

Although we can now conclude that the CSU GCM fails to simulate enough upper tropospheric clouds with a visible optical thickness less than 3.6 and has a tendency to form upper tropospheric clouds that are optically too thick, we further investigate the geographical distributions of thick and thin cirrus to determine which physical processes fundamental to the formation of optically thinner high-level clouds are missing or not realistically parameterized in the CSU GCM. Figure 12 show maps of the frequency of occurrence of thick and thin cirrus with cloud-top pressures less than 440 hPa in January and July.

Let us first concentrate on the geographical distribution of simulated thick cirrus relative to the satellite-derived cloud product. Comparing the top panels of Figure 12 against the bottom panels of Figures 5 and 7 reveals that setting aside the already established fact that the frequency of occurrence of tropical thick cirrus is strongly underestimated when compared against ISCCP-D1 data, the CSU GCM satisfactorily reproduces the geographical locations of the areas of maximum incidence of thick cirrus in July. Thick cirrus are simulated to form above the deep convective activity regions of Central America and equatorial Africa, as well as over the western Pacific and the Indian Oceans. On the other hand, the CSU GCM underestimates the amount of thick cirrus over a large portion of Asia and the southern part of North America, as well as across most of the Southern Ocean. Thick cirrus that extend over convectively active regions over the continents are not simulated as realistically for January as for July. In contrast to the observed thick cirrus, whose frequency of occurrence follows the seasonal shift of convection over land, the simulated thick cirrus remain locked in a July-like geographical distribution, with maxima located on each side of Central America and equatorial Africa. The GCM is more successful at reproducing the frequency of occurrence of thick cirrus over Asia in January than in July.

Next, we focus on the geographical distribution of the frequency of occurrence of thin cirrus. Comparison of the bottom panels of Figure 12 against the bottom panels of Figures 6 and 8 reveals strong differences between the model and observations in both months. In contrast to ISCCP-D1 data, which show that the optically thinnest clouds spread over a major part of the continents and consist of the smallest debris from convective outflow or are produced by orographic lifting, the CSU GCM forms thin cirrus preferably over the tropical oceans, outside of the main convectively active regions in January. It is also interesting to note that the amount of thin cirrus sharply

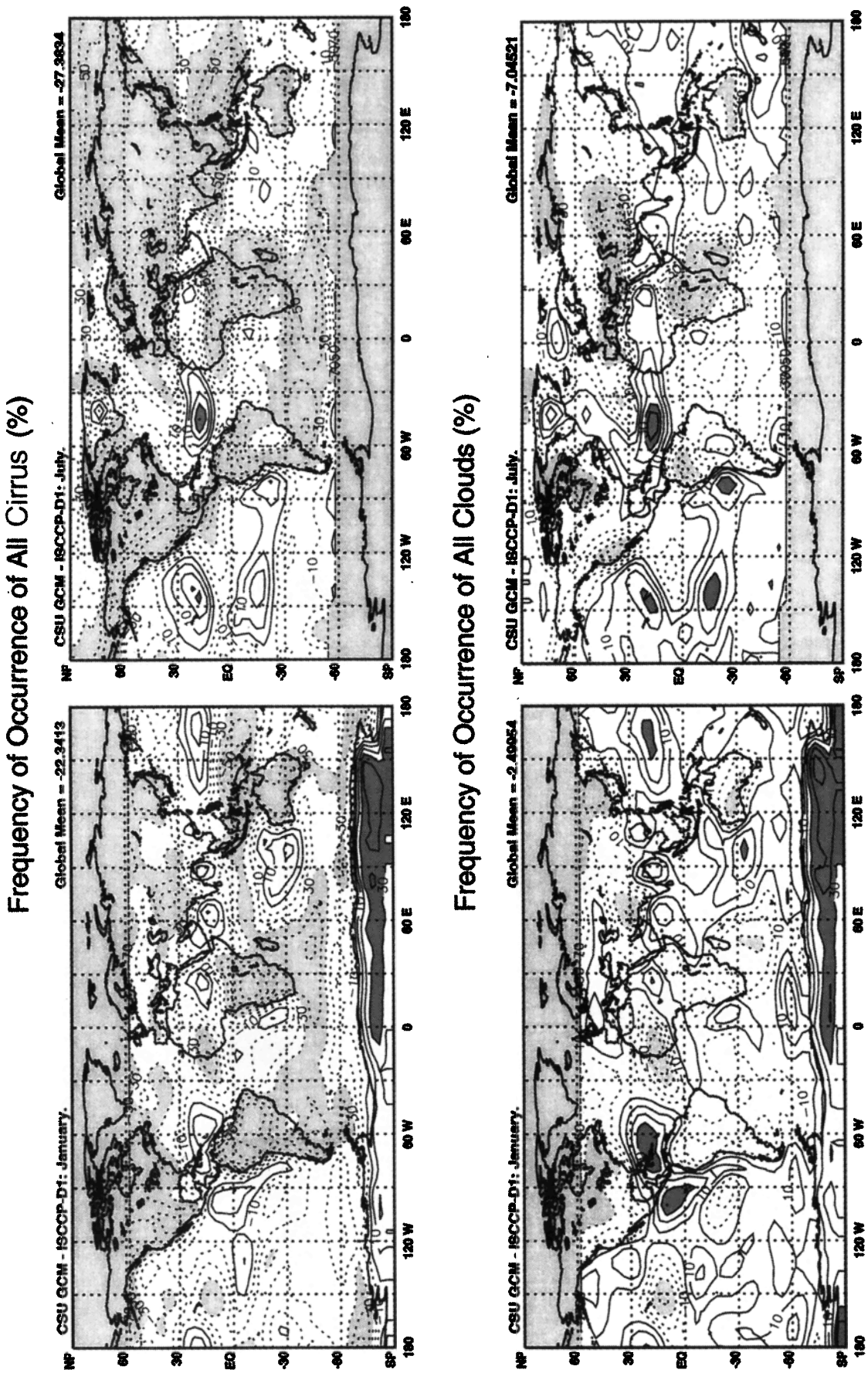

Figure 11. Geographical distribution of the difference between the frequency of occurrence of all cirrus and all clouds with cloud-top pressures less than 440 hPa simulated with the Colorado State University general circulation model (CSU GCM) against ISCCP-D1 data. Units are in percent, and contour intervals are every 10%. Light shading corresponds to differences less than −30%, and dark shading corresponds to differences greater than 30%.

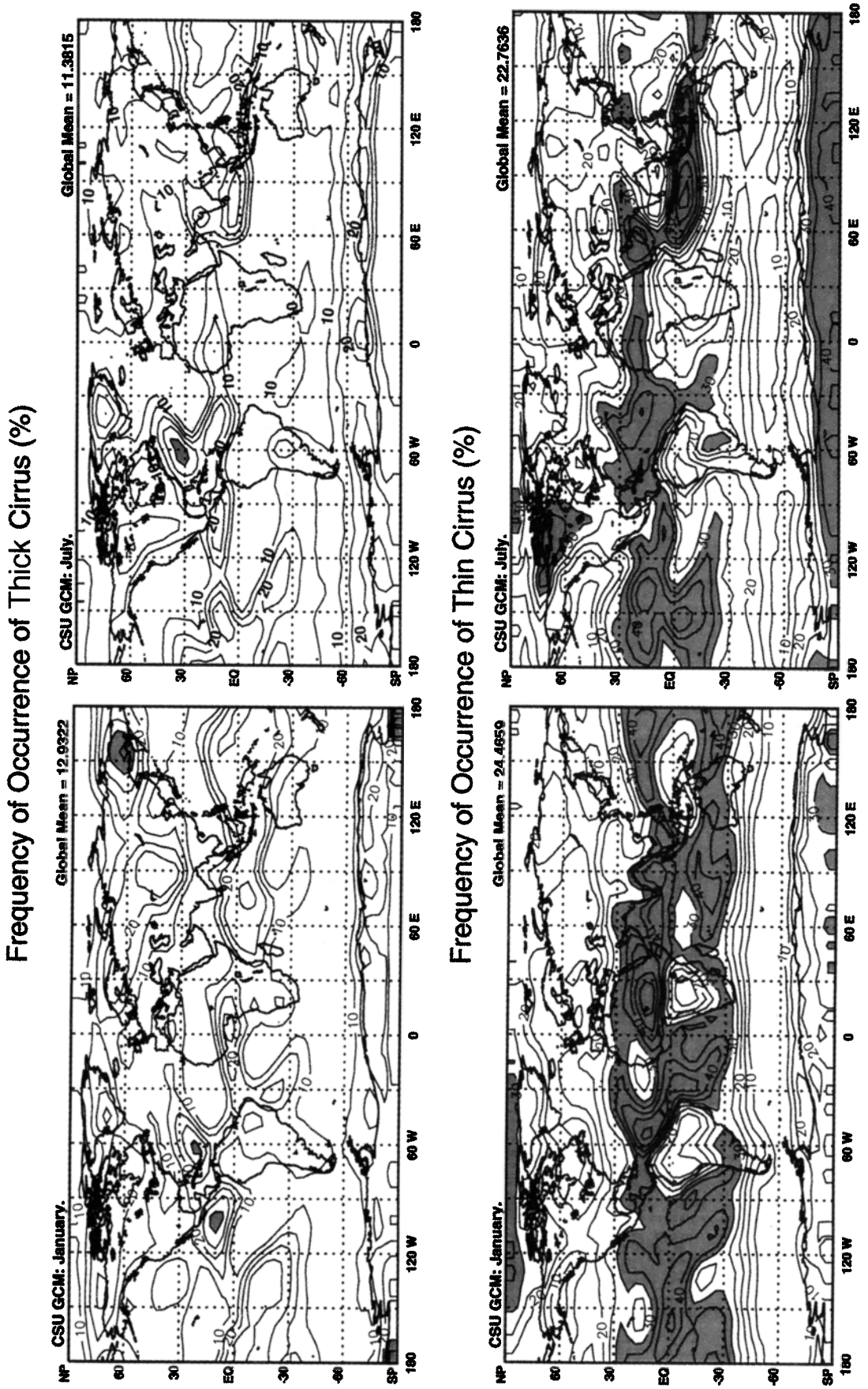

Figure 12. Geographical distribution of the frequency of occurrence of simulated (top panels) thick cirrus and (bottom panels) thin cirrus for cloud-top pressures less than 440 hPa, in (left panels) January and (right panels) July. Units are in percent, and contour intervals are every 10%. Shading corresponds to values greater than 30%.

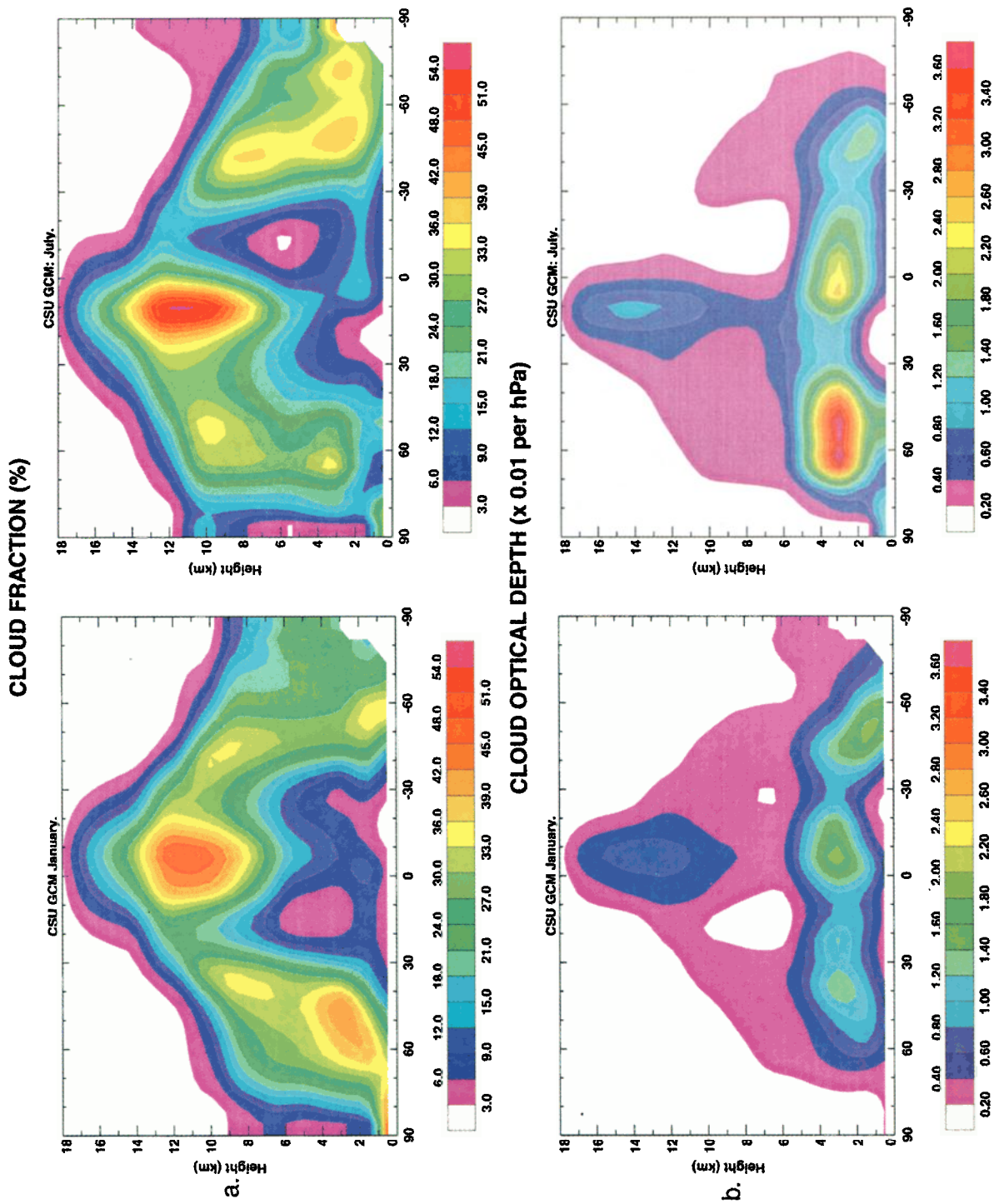

Plate 1. Latitude-versus-height cross sections of the zonally averaged (a) frequency of occurrence (in percent), and (b) optical depth (per hectopascals times 0.01) of cloudiness simulated with the CSU GCM. The left panels are for January, and the right panels are for July.

decreases in the middle and high latitudes in both January and July. As explained in section 3, simulated clouds can only form through detrainment of cloud water and cloud ice at the tops of cumulus updrafts or when the large-scale relative humidity exceeds 100%. Because thin cirrus are observed to form away from the chief convective centers, it is more likely that mechanisms that yield to their formation are supersaturation and horizontal advection of cloud ice. Comparison of the geographical distribution of thin cirrus against that of the cloud ice mixing ratio above 440 hPa reveals that areas of maximum cloud amounts coincide well with areas of minimum cloud ice mixing ratios. Maps of the cloud ice mixing ratio are omitted here for brevity. This makes sense since in the CSU GCM the optical depth of upper tropospheric clouds is proportional to the cloud ice mixing ratio. This relationship also explains the lesser amount of thin cirrus above the deep convective activity regions, where detrainment of cloud ice at the tops of cumulus towers is the most important source of cloud ice [*Fowler and Randall*, 1996]. The CSU GCM does not simulate a relationship between the physical process that triggers cloud formation and the corresponding preferred optical depths. The ISCCP-D1 data indicate that thick cirrus are mainly associated with convection, whereas thin cirrus are mainly associated with orographic lifting and large-scale advection. In contrast to the satellite-derived cloudiness, and as for the thick-cirrus category, there is little seasonal variation in the geographical distribution of thin cirrus.

5. Discussion

Results described in the previous section paint a bleak picture of the ability of the CSU GCM to reproduce the frequency of occurrence of upper tropospheric clouds with cloud-top pressures above 180, 310, and 440 hPa. The challenge now is to understand the origins of these discrepancies between the simulated and satellite-derived cloudiness and to propose ideas to improve the model's performance in the future. Let us first summarize the chief differences between simulated and satellite-derived upper tropospheric clouds.

1. The CSU GCM reproduces satisfactorily the zonally averaged distribution of upper tropospheric cloudiness when all ranges of τ are included but systematically underpredicts its frequency of occurrence for $\tau \leq 3.6$. We conclude that total-column optical depths for columns with high maximum cloud tops simulated with the CSU GCM are too thick relative to satellite-retrieved values.

2. The CSU GCM simulates tropical upper tropospheric clouds more successfully than upper tropospheric extratropical clouds. The model fails to simulate midlatitude upper tropospheric clouds over the continents, especially over elevated terrain and mountain ranges. In the tropics the formation mechanism for upper tropospheric clouds is mainly convection. In the middle latitudes, especially in winter, the primary formation mechanisms are frontal lifting in extratropical cyclones and orographic lifting over the major mountain ranges. The better simulation of tropical than extratropical cloudiness is understandable in view of the design of our current parameterization of cloud microphysics, in which we have an explicit mechanism for the formation of anvils by convective detrainment, while orographic and cyclone formation mechanisms are not formulated in such an explicit way. Because large-scale supersaturation is responsible for the formation of middle-latitude clouds and clouds are predicted to form if the relative humidity exceeds 100% [*Fowler et al.*, 1996], we need to focus our efforts on comparing the spatial distributions of the simulated temperature and water vapor mixing ratios against observations, especially over land. The coarse horizontal and vertical resolutions of the CSU GCM also contribute to the poor simulation of upper tropospheric clouds in extratropical cyclones and hinder the formation of thin cirrus by orographic lifting.

Several factors can contribute to the discrepancies between the columnar optical depths simulated by the CSU GCM and those retrieved from ISCCP satellite radiances. First, it is important to keep in mind that the satellite-retrieved optical depths are themselves model-dependent quantities and that the cloud parameterization used to retrieve the ISCCP-D1 cloud products is very different from that used in the CSU GCM. As mentioned earlier, satellite-derived optical depths are obtained using a radiative transfer model that adjusts the optical depth values until the computed visible radiances match the corresponding measured radiances. In a sense, the strategy used to retrieve optical depths from satellite radiances is the opposite of that used to compute optical depths in a GCM. In a GCM the computations of cloud optical properties and radiative fluxes are based upon a priori information about the cloud water paths, whereas satellite-derived optical depths and water paths result from earlier measurements of top-of-the-atmosphere radiances. In particular, the radiative transfer model that retrieves satellite optical depths does not account for multilayered cloud systems and assumes that the cloud thickness is contained in a contiguous layer and that atmospheric gases are contained in the layers above or below the cloud layer (W. Rossow, personal communication, 1998). It is equally important to remember that ISCCP-D1 optical depths are first computed at the pixel level before being spatially averaged on equal-area grids with a 280-km resolution. This is in contrast to simulated optical depths, which are computed using grid-averaged cloud liquid and ice paths using the assumption that the horizontal area covered by clouds is equal to that of the model grid box.

Up to this point, nothing has been said about the total-column optical depth (τ_T) and the vertical distribution of clouds and their optical properties in the CSU GCM. January and July maps of τ_T from ISCCP-D1 data show that above convectively active areas, monthly-averaged τ_T ranges between 6 and 8. In contrast, simulated values of τ_T reach values in excess of 20 in the same regions (maps of simulated and satellite-observed τ_T are omitted here for brevity), confirming that the simulated total-column optical depth is too large relative to the observations. Plate 1 shows that in the tropics the optical depth of low-level clouds is greater than that of upper tropospheric clouds and contributes a major part to the total column optical depth, although the frequency of occurrence of clouds is maximum in the upper troposphere. As seen in Plate 1, the optical depth of clouds below 4 km reaches values in excess of 0.02 per hPa, whereas that of clouds above 10 km is less than 0.008 per hPa. Above convectively active regions where, on a monthly average, low-level and upper tropospheric clouds are predicted to form simultaneously, the optical depth of low-level clouds contributes a substantial fraction of the total-column optical depth. If the simulated optical depth of low-level clouds was less than that seen in Plate 1, the total-column optical depth would be closer to that derived from ISCCP-D1 data, and the simulated frequency of occurrence of all cirrus relative to that of all clouds would increase. *Fowler*

and Randall [1996] demonstrate that over tropical convectively active regions the planetary albedo simulated with the CSU GCM is too high relative to ERBE data. Reducing the simulated optical depth of low-level clouds would also help correct that discrepancy.

This finding highlights important limitations in using ISCCP-D1 cloud products or any other cloud climatology derived from top-of-the-atmosphere radiances when multilevel cloud systems are present, as is the case in tropical regions of deep convection. Because information on the base levels of individual cloud layers is not available in the observations, it has to be assumed that the satellite-derived optical depth is that of a single-layer cloud, regardless of the actual vertical distribution of the cloud layers. This assumption seriously hampers our ability to accurately identify the origins of the discrepancies between the model results and satellite data. By using the satellite-observed total-column atmospheric optical depth and the frequency of occurrence of upper tropospheric clouds, we have inferred that the optical depths of the simulated low-level clouds are too high. Additional hypotheses are proposed below. An increased observational basis for understanding of the overlapping of multilayer cloud systems, as discussed by *Hahn et al.* [1982], *Tian and Curry* [1989], and *Wang and Rossow* [1995], is sorely needed. Until then, it will remain difficult to assess the ability of GCMs to simulate the optical properties of anvils above the convectively active regions of the tropics.

In order to further understand the inability of the CSU GCM to simulate optically thin upper tropospheric clouds, we investigate the global distribution of clouds with cloud tops less than 180 hPa and $\tau \leq 1.6$, with no clouds underneath. In doing so, our comparison of the thinnest clouds simulated by the CSU GCM against ISCCP-D1 data is more readily interpretable. Diagnostics show that the globally averaged difference between the frequency of occurrence of thin cirrus with and without clouds underneath is equal to 2.1% in January and 2.5% in July, suggesting that simulated thin cirrus are mostly single-layer clouds that are indeed optically too thick.

From (1) we see that the excessive simulated cloud optical depth, relative to the ISCCP-D1 retrieved value, may be due to some combination of the following causes: (1) The formulation of τ as a function of the ice water path is improper for upper tropospheric clouds; (2) the simulated ice water content in upper tropospheric clouds is unrealistically large; (3) the value chosen for the effective radius is too small; and/or (4) the geometrical thickness of the model layers is too large to allow simulation of optically thin cloud layers.

Equation (1) provides a convenient approach to compute the broadband optical thickness of clouds in GCMs because it requires only the liquid or ice water content and effective radius as input parameters. Using different values of r_e to distinguish between the size of water droplets and ice crystals, (1) can be used to calculate the optical thickness of both water and ice clouds in GCMs [*Del Genio et al.*, 1996; *Fowler and Randall*, 1996; *Rotstayn*, 1997]. Equation (1) implicitly assumes, however, that ice crystals are spherical and that their radius is large with respect to solar wavelengths so that Mie theory applies [*Stephens*, 1978].

Because the optical depth is a linear function of the cloud ice path, it is natural to suspect that excessive ice water contents are responsible for increased simulated optical depths. This hypothesis is difficult to test using the available data. As discussed by *Fowler et al.* [1996], it is impossible to compare the geographical distribution of the ice water path simulated by the CSU GCM against observations because the amount of cloud ice suspended in the atmosphere remains completely unknown, except for the preliminary estimates of *Lin and Rossow* [1994] for nonprecipitating clouds. In the CSU GCM, cloud microphysics parameters such as the autoconversion thresholds of cloud water to rain and cloud ice to snow, and the collection efficiency factors of rain to collect cloud liquid water and of snow to collect cloud liquid and ice water, were tuned so that the globally averaged radiative forcing of clouds at infrared and solar wavelengths agree reasonably well with ERBE data. Until the global distributions of the cloud liquid and ice water paths are known from observations, it will remain difficult to assess the ability of cloud microphysics parameterizations used in GCMs to simulate interactions among the atmospheric hydrologic cycle, clouds, and radiation.

The effective radius is a convenient parameter that can be used to describe the scattering properties of water and ice clouds [*McFarquhar and Heymsfield*, 1998] and can be easily included in climate models [*Ebert and Curry*, 1992; *Slingo*, 1989]. A wide variety of values has been suggested for the effective radius of ice crystals, ranging from 16 μm [*Stephens et al.*, 1990] to 50 μm [*Francis et al.*, 1994]. Refined parameterizations of the effective radius in terms of the ice/water content in tropical and frontal cirrus clouds are also being developed [*Platt*, 1997]. As for the cloud microphysics parameters, the value of the effective radius was prescribed so that the globally averaged top-of-the atmosphere longwave and shortwave radiative fluxes were in good agreement with ERBE data.

Finally, we want to address the impact of the model's vertical resolution on the simulation of visible optical depths.

The Lidar In-Space Technology Experiment (LITE) [*McCormick et al.*, 1993], flown on the space shuttle *Discovery* as part of the STS-64 mission between September 9 and 20, 1994, offered a unique opportunity to study the geometrical characteristics and optical properties of multilayered cloud systems on a 250-km scale [*Winker*, 1997]. One major objective of LITE was to provide a unique and complementary data set on the properties of individual cloud layers that cannot be readily obtained from a cloud climatology data set such as ISCCP. Figure 13 shows (left panels) the histograms and (right panels) cumulative probability distributions of the geometrical thickness of cloudy layers estimated from LITE data. The top panels display the statistical properties of cloudy layers regardless of their cloud-top heights. The bottom panels display the properties of cloudy layers with cloud-top heights greater than 8 km, limiting the statistical distribution to that of upper tropospheric clouds only. The LITE data reveal that the geometrical thickness of individual cloudy layers, including that of upper tropospheric clouds, is typically of the order of 200 m. The number of cloudy layers decreases sharply for geometrical thicknesses greater than 200 m. As seen in Figure 13, the cumulative probability distributions of the geometrical thickness of all clouds and upper tropospheric clouds reach their asymptotic values for thicknesses greater than 4000 m. When all cloud-top heights are considered, about half of the LITE cloud layers are less than 1 km thick. For clouds with cloud-top heights greater than 8 km, we found that 50% of the LITE cloud layers are about 1.4 km thick.

Except for PBL clouds, clouds simulated with the CSU GCM are assumed to vertically fill the atmospheric layer in which they are predicted to form, constraining their geometrical thicknesses to be equal to those prescribed by the vertical

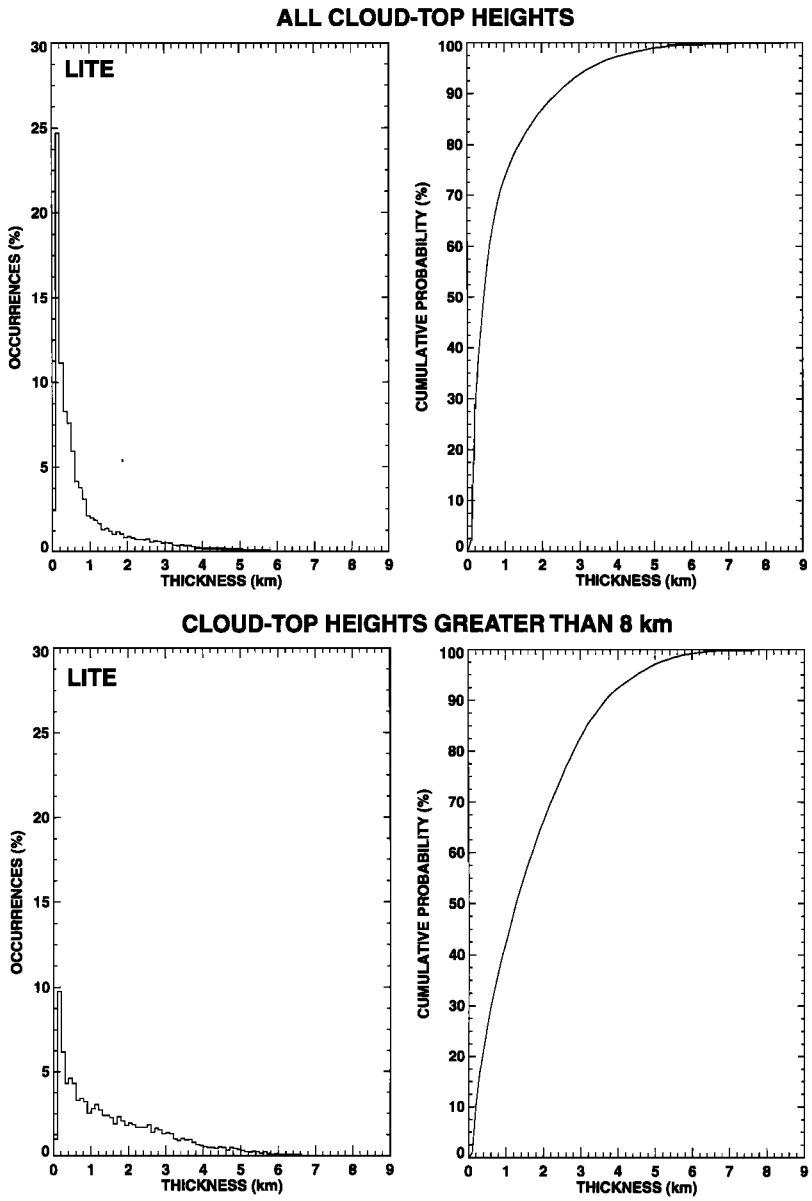

Figure 13. Histograms and cumulative probability distributions of the geometrical thickness of cloudy layers measured by the Lidar In-Space Technology Experiment (LITE).

discretization. The vertical discretization is based on a modified σ coordinate in which the PBL is the bottom layer of the model [*Suarez et al.*, 1983]. The free troposphere defined between the top of the PBL and the tropopause includes 14 layers. Between the PBL top with pressure p_B and p_I = 100 hPa, the vertical coordinate is defined as

$$\sigma = \left(\frac{p_B - p}{\pi_L}\right) \qquad (p_B \geq p \geq p_I) \tag{2}$$

where $\pi_L = p_B - p_I$ is the pressure thickness of the "troposphere." Using the monthly-averaged PBL top pressure and vertical distribution of the monthly-averaged temperature, we computed the statistical distribution of the geometrical thickness of tropospheric layers above the PBL. Figure 14 is the same as Figure 13 but for the geometrical thickness of cloudy layers simulated in the CSU GCM. Figure 14 reveals that the minimum geometrical thickness of individual simulated cloud layers is of the order of 1000 m, or much larger than many of the observed cloud-layer thicknesses. This means that for a given ice water path and given effective radius, the optical depth of a single cloud layer would be underestimated by a factor of 5 when using (1), relative to the one that would be obtained if the GCM layer thicknesses had the same magnitude as the thicknesses derived from LITE data. The problem of systematically overestimating the cloud optical depth and underestimating the cloud cover in GCMs in which vertical resolutions are too coarse and clouds are assumed to fill the entire model layer has been addressed by *Del Genio et al.* [1996]. Under stable conditions and for radiative purposes only, *Del Genio et al.* [1996] choose to distribute the cloud fraction evenly in three dimensions, allowing the cloud physical thickness to be less than that of the model thickness. However, until the vertical resolution of the CSU GCM is increased, the simulation of the optically and geometrically thin clouds ob-

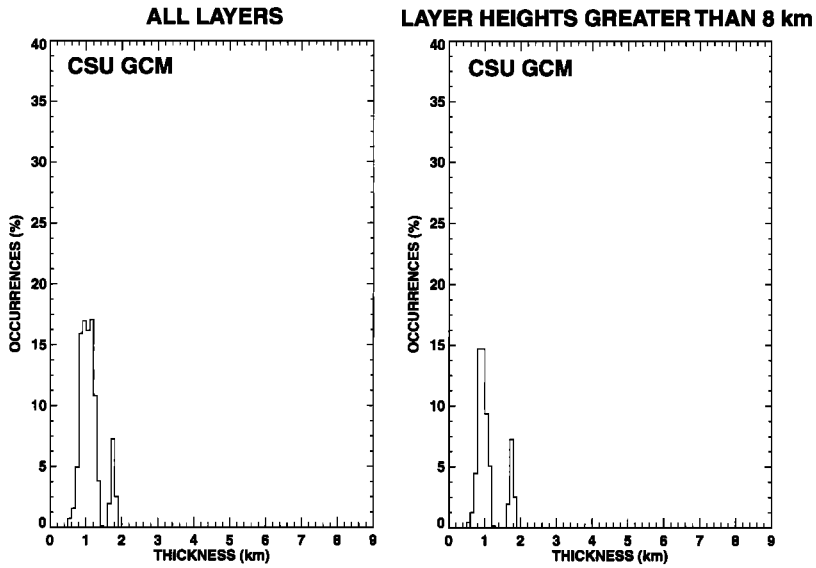

Figure 14. Same as Figure 13, but for cloudy layers in the CSU GCM.

served in the ISCCP-D1 data and the SAGE II [*Kent et al.*, 1993] and HIRS [*Wylie et al.*, 1994] cloud climatologies will remain difficult, regardless of the parameterizations of cloud microphysics and radiative processes. This provides a strong motivation to increase the number of layers used in the GCM.

6. Summary

The objective of our study was to compare the chief deficiencies in simulating upper tropospheric clouds with the CSU GCM against ISCCP-D1 cloud data. To do so, we designed model diagnostics as close as possible to the ones available from observations, allowing us to compare the frequency of occurrence of upper tropospheric clouds for various ranges of visible cloud optical depths. Differences in the geographical distributions of thick and thin cirrus clouds were discussed from the model and satellite data. Comparing the geographical distribution and optical properties of upper tropospheric clouds simulated with the CSU GCM against ISCCP-D1 cloud products revealed significant failures in several aspects of our parameterization of cloudiness.

The more realistic simulation of tropical than extratropical upper tropospheric cloudiness provides incentives to investigate and revise formation mechanisms of cloudiness in the middle latitudes, not only over the oceanic storm track regions but also over the continents. Because large-scale saturation is the chief mechanism for cloud production in the extratropics, we plan to analyze the distributions of water vapor, temperature, and relative humidity and to study the effects of increased horizontal and vertical resolutions on the triggering of frontal lifting in extratropical cyclones. The difficulty of simulating upper tropospheric clouds has recently been discussed by *Rotstayn* [1998] and *Hack et al.* [1998] using climate simulations that included fractional cloudiness. A January zonally averaged distribution of the high-level cloud fraction obtained with the Commonwealth Scientific and Industrial Research Organization (CSIRO) GCM revealed that like the CSU GCM, the CSIRO model simulated tropical more satisfactorily than extratropical high-level clouds when compared against both HIRS and ISCCP-D2 cloud data [*Rotstayn*, 1998, Figure 2.c). In the middle latitudes, simulated upper tropospheric clouds were overestimated relative to the satellite data, while in the tropics the zonally averaged fraction of high-level clouds was underestimated in the CSIRO climate simulations. Like the CSU GCM, the CSIRO climate simulations suffer from a lack of upper tropospheric clouds over land along the ITCZ and the northern hemisphere middle latitudes, suggesting that the simulated upper troposphere was too dry [*Rotstayn*, 1998, Figure 8). The sensitivity of upper tropospheric clouds to the parameterization of deep convection was briefly discussed by *Hack et al.* [1998]. Comparing Version 3 (CCM3) against Version 2 (CCM2) of the NCAR Community Climate Model showed a 5.1% increase in the globally averaged high-level cloud fraction when the parameterization of deep cumulus convection of *Zhang and McFarlane* [1995] is added to the original scheme of *Hack* [1994].

Results show that the increased frequency of occurrence of simulated all cirrus relative to that of all clouds results in part because the classification of upper tropospheric clouds between thin and thick cirrus is based upon the total column optical depth, which is overestimated in the CSU GCM. Comparison between the simulated and satellite-derived total-column optical depth suggests that the optical depth of low-level clouds may be overestimated in the model, but this hypothesis is difficult to test using available data. One major limitation in using satellite-derived cloud climatologies such as ISCCP-D1 cloud products to understand the role of upper tropospheric clouds in GCMs is that the observational products do not provide any information on the vertical distributions of the cloudiness and its optical thickness. In addition to conventional satellite experiments such as ERBE and ISCCP, which provide top-of-the-atmosphere global distributions of the Earth radiation budget and cloudiness, additional lidar- and radar-in-space missions are needed to increase our understanding of multilayer cloud systems.

The ability of the CSU GCM in the simulation of upper tropospheric cloudiness will need to be reevaluated when the model has been modified to include a parameterization of the fractional cloudiness. As explained in section 2, an arbitrary

Table 3. Globally Averaged Frequency of Occurrence of Simulated Upper Tropospheric Clouds by Cloud Type, for January and July

	January			July		
Cloud Type	180 hPa	310 hPa	440 hPa	180 hPa	310 hPa	440 hPa
All clouds	25.4	54.3	61.9	26.8	52.1	58.9
All cirrus	15.7	32.9	37.4	15.6	30.2	34.1
Thick cirrus	5.0	10.8	13.0	4.9	9.7	11.4
Thin cirrus	10.7	22.1	24.5	10.7	20.5	22.8

Values are given in percent.

threshold of the liquid/ice water content is used to avoid the formation of clouds with a 100% cloud fraction associated with small mixing ratios of cloud water and ice. This arbitrary threshold was introduced to avoid the formation of optically thin clouds, mainly over desert regions and cloud-free subtropical oceans. Once the model allows the cloud fraction to continuously vary between 0 and 1, this threshold will become unnecessary, since the coupling between the parameterizations of fractional cloudiness and cloud microphysical processes will automatically relate the horizontal cloud fraction to the grid-cell-averaged water/ice content. The effect of the liquid water/ice content threshold is to reduce the globally averaged cloud statistics listed in Tables 2 and 3. In a sense, the threshold acts in the same manner as a fractional cloudiness, which would also remove clouds with small liquid/ice mixing ratios under subsaturated conditions. The inclusion of fractional cloudiness will also allow us to assess the model performance to simulate upper tropospheric clouds against observations directly in terms of cloud amounts instead of frequencies of occurrence.

Further investigation of the discrepancies between the CSU GCM and satellite data should focus not only on the vertical distribution and magnitude of the ice water path and cloudiness, but also on the vertical discretization of the simulated atmosphere. Results show that because the geometrical thickness of cloudy layers is set equal to that of the model layers, it is important to increase the vertical resolution used in GCMs so that model layers are of the order of 200 m thick (or thinner), as suggested from the analysis of LITE data. We plan to run a set of experiments to further investigate the impact of vertical resolution on the simulation of optically thin upper tropospheric clouds in the CSU GCM.

Acknowledgments. This research was sponsored by the National Science Foundation under grant ATM-8907414 and by NASA under grant NAG-1-1266 and contract NAS-1-19951, all to Colorado State University. Computing resources were provided by the Scientific Computing Division at the National Center for Atmospheric Research, by the National Center for Computational Sciences at NASA Goddard, and by the National Energy Research Supercomputer Center at Lawrence Livermore National Laboratory. We thank David Winker and M. Patrick McCormick for providing the LITE data. The ISCCP-D1 data were obtained from the NASA Langley Research Center's EOS-DIS Distributed Active Archive Center.

References

Arakawa, A., and W. H. Schubert, The interactions of a cumulus cloud ensemble with the large-scale environment, I, *J. Atmos. Sci.*, *31*, 674–701, 1974.

Barkstrom, B. R., The Earth Radiation Budget Experiment (ERBE), *Bull. Am. Meteorol. Soc.*, *65*(11), 1170–1185, 1984.

Boucher, O., H. Le Treut, and M. B. Baker, Precipitation and radiation modeling in a GCM: Introduction of cloud microphysical processes, *J. Geophys. Res.*, *100*, 16,395–16,414, 1995.

Del Genio, A. D., M.-S. Yao, W. Kovari, and K. K. W. Lao, A prognostic cloud water parameterization for global climate models, *J Clim.*, *9*, 270–304, 1996.

Ding, P., and D. A. Randall, A cumulus parameterization with multiple cloud base levels, *J. Geophys. Res.*, *103*, 11,341–11,353, 1998.

Ebert, E. E., and J. A. Curry, A parameterization of ice cloud optical properties for climate models, *J. Geophys. Res.*, *97*, 3831–3836, 1992.

Fowler, L. D., and D. A. Randall, Liquid and ice cloud microphysics in the CSU general circulation model, II, Impact on cloudiness, the Earth's radiation budget, and the general circulation of the atmosphere, *J. Clim.*, *9*, 530–560, 1996.

Fowler, L. D., D. A. Randall, and S. A. Rutledge, Liquid and ice cloud microphysics in the CSU general circulation model, I, Model description and simulated cloud microphysical processes, *J. Clim.*, *9*, 489–529, 1996.

Francis, P. N., A. Jones, R. W. Saunders, K. P. Shine, A. Slingo, and Z. Sun, An observational and theoretical study of the radiative properties of cirrus: Some results from ICE'89, *Q. J R. Meteorol. Soc.*, *120*, 809–848, 1994.

Greenwald, T. J., G. L. Stephens, T. H. Vonder Haar, and D. L. Jackson, A physical retrieval of cloud liquid water over the global oceans using special sensor microwave/imager (SSM/I) observations, *J. Geophys. Res.*, *98*, 18,471–19,488, 1993.

Hack, J. J., Parameterization of moist convection in the National Center for Atmospheric Research Community Climate Model (CCM2), *J. Geophys. Res.*, *99*, 5551–5568, 1994.

Hack, J. J., J. T. Kiehl, and J. W. Hurrell, The hydrologic and thermodynamic characteristics of the NCAR CCM3, *J. Clim.*, *11*, 1179–1206, 1998

Hahn, C. J., S. G. Warren, J. London, R. M. Chervin, and R. Jenne, Atlas of simultaneous occurrence of different cloud types over the ocean, *NCAR Tech. Note TN-201+STR NCAR*, Natl. Cent. for Atmos. Res., Boulder, Colo., 1982.

Harshvardhan, D. A. Randall, T. G. Corsetti, and D. A. Dazlich, Earth radiation budget and cloudiness simulations with a general circulation model, *J. Atmos. Sci.*, *46*, 1922–1942, 1989.

Jin, Y., W. B. Rossow, and D. P. Wylie, Comparison of the climatologies of high-level clouds from HIRS and ISCCP, *J. Clim.*, *9*, 2850–2879, 1996.

Kent, G. S., D. M. Winker, M. T. Osborn, M. P. McCormick, and K. M. Skeens, A model for the separation of cloud and aerosol in SAGE II occultation data, *J. Geophys. Res.*, *98*, 20,725–20,735, 1993.

Liao, X., W. B. Rossow, and D. Rind, Comparison between SAGE II and ISCCP high-level clouds, 1, Global and zonal mean cloud amounts, *J Geophys Res.*, *100*, 1121–1135, 1995.

Lin, B., and W. B. Rossow, Observations of cloud liquid water path over the oceans: Optical and microwave remote sensing methods, *J. Geophys. Res.*, *99*, 20,907–20,928, 1994.

Lord, S. J., Interaction of a cumulus cloud ensemble with the large-scale environment, III, Semi-prognostic tests of the Arakawa-Schubert cumulus parameterization, *J. Atmos. Sci.*, *39*, 88–103, 1982.

Lord, S. J., W. C. Chao, and A. Arakawa, Interaction of a cumulus cloud ensemble model with the large-scale environment, IV, The discrete model, *J. Atmos. Sci.*, *39*, 104–113, 1982.

McClatchey, R. A., R. W. Fenn, J. E. A. Selby, F. E. Volz, and J. S. Garing, Optical properties of the atmosphere, *AFCRL-72-0497, Environ Res Pap. 411*, Air Force Cambridge Res. Lab., Hanscom Air Force Base, Mass., 1972.

McCormick, M. P., et al., Scientific investigations planned for the Lidar In-Space Technology Experiment (LITE), *Bull. Am. Meteorol. Soc.*, *74*, 205–214, 1993.

McFarquhar, G. M., and A. J. Heymsfield, The definition and significance of an effective radius, *J. Atmos. Sci.*, *55*, 2039–2052, 1998.

Minnis, P., K.-N. Liou, and Y. Takano, Inference of cirrus cloud properties using satellite-observed visible and infrared radiances, I, Parameterization of radiance fields, *J. Atmos. Sci.*, *50*, 1279–1304, 1993a.

Minnis, P., P. W. Heck, and D. F. Young, Inference of cirrus cloud properties using satellite-observed visible and infrared radiances, II, Verification of theoretical cirrus radiative properties, *J. Atmos. Sci.*, *50*, 1305–1322, 1993b.

Pan, D.-M., and D. A. Randall, A cumulus parameterization with a prognostic closure, *Q. J. R. Meteorol. Soc.*, *124*, 949–981, 1998.

Platt, C. M. R., A parameterization of the visible extinction coefficient of ice clouds in terms of the ice/water content, *J. Atmos. Sci.*, *54*, 2083–2098, 1997.

Ramanathan, V., E. J. Pitcher, R. C. Malone, and M. L. Blackmon, The response of a general circulation model to refinements in radiative processes, *J. Atmos. Sci.*, *40*, 605–630, 1983.

Ramaswamy, V., and V. Ramanathan, Solar absorption by cirrus clouds and the maintenance of the tropical upper-tropospheric thermal structure, *J. Atmos. Sci.*, *46*, 2293–2310, 1989.

Ricard, J. L., and J. F. Royer, A statistical scheme for use in an AGCM, *Ann. Geophys.*, *11*, 1095–1115, 1993.

Rossow, W. B., and L. C. Garder, Cloud detection using satellite measurements of infrared and visible radiances for ISCCP, *J. Clim.*, *6*, 2341–2369, 1993a.

Rossow, W. B., and L. C. Garder, Validation of ISCCP cloud detections, *J. Clim.*, *6*, 2370–2393, 1993b.

Rossow, W. B., A. W. Walker, D. E. Beuschel, and M. D. Roiter, International Satellite Cloud Climatology Project (ISCCP) documentation of new cloud data sets, *WMO/TD-No. 737*, 115 pp., World Meteorol. Organ., Geneva, 1996.

Rotstayn, L. D., A physically-based scheme for the treatment of stratiform clouds and precipitation in large-scale models, I, Description and evaluation of microphysical processes, *Q. J. R. Meteorol. Soc.*, *123*, 1227–1282, 1997.

Rotstayn, L. D., A physically-based scheme for the treatment of stratiform clouds and precipitation in large-scale models, II, Comparison of modelled and observed climatological fields, *Q. J. R. Meteorol. Soc.*, *124*, 389–415, 1998.

Schiffer, R. A., and W. B. Rossow, The International Satellite Cloud Climatology Project (ISCCP): The first project of the World Climate Research Program, *Bull. Am. Meteorol. Soc.*, *64*, 779–784, 1983.

Schiffer, R. A., and W. B. Rossow, ISCCP cloud data products, *Bull. Am. Meteorol. Soc.*, *72*, 2–20, 1991.

Senior, C. A., and J. F. B. Mitchell, Carbon dioxide and climate: The impact of cloud parameterization, *J. Clim.*, *6*, 393–418, 1993.

Simpson, J., R. A. Adler, and G. R. North, A proposed Tropical Rainfall Measuring Mission (TRMM) satellite, *Bull. Am. Meteorol. Soc.*, *69*, 275–295, 1988.

Slingo, A., A GCM parameterization for the shortwave radiative properties of water clouds, *J. Atmos. Sci.*, *46*, 1419–1427, 1989.

Slingo, A., and J. M. Slingo, The response of a general circulation model to cloud longwave radiative forcing, I, Introduction and initial experiments, *Q. J. R. Meteorol. Soc.*, *114*, 1027–1062, 1988.

Smith, R. N. B., A scheme for predicting layer clouds and their mass content in a general circulation model, *Q. J. R. Meteorol. Soc.*, *116*, 435–460, 1990.

Stephens, G. L., Radiation profiles in extended water clouds, II, Parameterization schemes, *J. Atmos. Sci.*, *35*, 2123–2132, 1978.

Stephens, G. L., S.-C. Tsay, P. W. Stackhouse, and P. J. Flatau, The relevance of the cloud microphysical and radiative properties of cirrus clouds to climate and climate feedbacks, *J. Atmos. Sci.*, *47*, 1742–1753, 1990.

Suarez, M. J., A. Arakawa, and D. A. Randall, Parameterization of the planetary boundary layer in the UCLA general circulation model: Formulation and results. *Mon. Weather Rev.*, *111*, 2224–2243, 1983.

Tian, L., and J. A. Curry, Cloud overlap statistics, *J. Geophys. Res.*, *94*, 9925–9935, 1989.

Tiedtke, M., Representation of clouds in large-scale models, *Mon. Weather Rev.*, *121*, 3040–3061, 1993.

Wang, J. W., and W. B. Rossow, Determination of cloud vertical structure from upper-air observations, *J. Appl. Meteorol.*, *34*, 2243–2258, 1995.

Wang, P.-H., P. Minnis, M. P. McCormick, G. S. Kent, and K. M. Skeens, A 6-year climatology of cloud occurrence frequency from SAGE II observations (1985–1990), *J. Geophys. Res.*, *101*, 29,407–29,429, 1996.

Weng, F., N. C. Grody, R. Ferraro, A. Batist, and D. Forsyth, Cloud liquid water climatology from the special sensor microwave imager, *J. Clim.*, *10*, 1086–1098, 1997.

Wielicki, B. A., B. R. Barkstrom, E. F. Harrison, R. B. Lee III, G. L. Smith, and J. E. Cooper, Clouds and the Earth's Radiant Energy System (CERES): An Earth observing system experiment, *Bull. Am. Meteorol. Soc.*, *77*, 853–868, 1996.

Winker, D. M., Observations of the vertical distribution of clouds using space lidar, in *Proceedings of the 9th AMS Conference on Atmospheric Radiation*, pp. 422–425, Am. Meteorol. Soc., Boston, Mass., 1997.

World Meteorological Organization, Workshop in cloud microphysics parameterizations in global atmospheric circulation models, *WMO/TD-No. 713*, Geneva, 1995.

Wylie, D. P., H. M. Woolf, and K. I. Strabala, Four years of global cirrus cloud statistics using HIRS, *J. Clim.*, *7*, 1972–1986, 1994.

Zhang, G. J., and N. A. McFarlane, Sensitivity of climate simulations to the parameterization of cumulus convection in the Canadian Climate Centre general circulation model, *Atmos. Ocean*, *33*, 407–446, 1995.

L. D. Fowler and D. A. Randall, Department of Atmospheric Science, Colorado State University, Fort Collins, CO 80523. (laura@slikrock.atmos.colostate.edu)

(Received June 20, 1998; revised October 23, 1998; accepted October 27, 1998.)